ACS Infectious Diseases

pubs.acs.org/journal/aidcbc Article

# Discovery of Prenyltransferase Inhibitors with *In Vitro* and *In Vivo* Antibacterial Activity

Junfeng Song, Satish R. Malwal, Noman Baig, Lici A. Schurig-Briccio, Zijun Gao, Girija S. Vaidya, Kailing Yang, Nader S. Abutaleb, Mohamed N. Seleem, Robert B. Gennis, Taras V. Pogorelov, Eric Oldfield,* and Xinxin Feng*

Cite This: https://dx.doi.org/10.1021/acsinfecdis.0c00472 Read Online

ACCESS | Metrics & More | Article Recommendations | Supporting Information

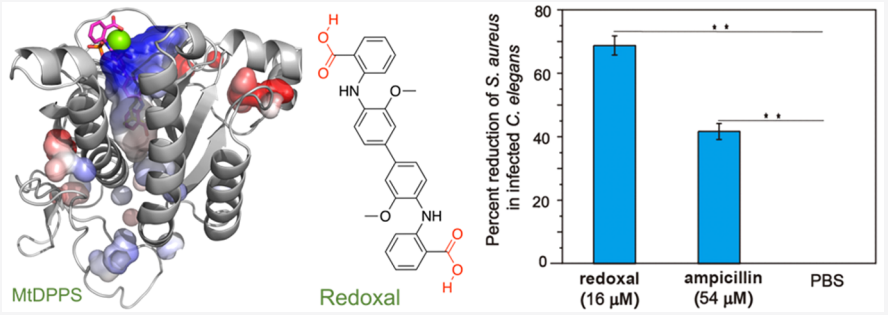


**ABSTRACT:** *Cis*-prenyltransferases such as undecaprenyl diphosphate synthase (UPPS) and decaprenyl diphosphate synthase (DPPS) are essential enzymes in bacteria and are involved in cell wall biosynthesis. UPPS and DPPS are absent in the human genome, so they are of interest as targets for antibiotic development. Here, we screened a library of 750 compounds from National Cancer Institute Diversity Set V for the inhibition of *Mycobacterium tuberculosis* DPPS and found 17 hits, and then $IC_{50}$s were determined using dose−response curves. Compounds were tested for growth inhibition against a panel of bacteria, for *in vivo* activity in a *Staphylococcus aureus*/*Caenorhabditis elegans* model, and for mammalian cell toxicity. The most active DPPS inhibitor was the dicarboxylic acid redoxal (compound **10**), which also inhibited undecaprenyl diphosphate synthase (UPPS) as well as farnesyl diphosphate synthase. **10** was active against *S. aureus*, *Clostridiodes difficile*, *Bacillus anthracis* Sterne, and *Bacillus subtilis*, and there was a 3.4-fold increase in $IC_{50}$ on addition of a rescue agent, undecaprenyl monophosphate. We found that **10** was also a weak protonophore uncoupler, leading to the idea that it targets both isoprenoid biosynthesis and the proton motive force. In an *S. aureus*/*C. elegans in vivo* model, **10** reduced the *S. aureus* burden 3 times more effectively than did ampicillin.

**KEYWORDS:** *cis-prenyltransferases, growth inhibition, DPPS inhibitor, $IC_{50}$, S. aureus, antibiotics*



## INTRODUCTION

Developing antibiotics with new mechanisms of action is important in order to help combat drug resistance. However, many new antibiotics in the clinical pipeline are modifications of old antibiotics, according to the *Antimicrobial Agents in Clinical Development Report* issued by the World Health Organization in 2017,[1] and resistance typically occurs quite rapidly. Moreover, drugs with truly novel mechanisms of action tend to be held in reserve lest they lose efficacy due to resistance development. It is thus clear that many new targets and inhibitors are needed, and multitarget inhibitors might be advantageous from a resistance-development perspective.

The bacterial cell wall biosynthesis pathway is an attractive target for new inhibitors since several clinically important antibiotics, such as β-lactams, vancomycin, fosfomycin, and bacitracin,[2] inhibit this pathway. An early step in cell wall biosynthesis in most bacteria involves the condensation of isopentenyl diphosphate (IPP, **1**, Figure 1a) and dimethylallyl diphosphate (DMAPP, **2**) to form (via geranyl diphosphate) all *trans*-farnesyl diphosphate (FPP, **3**), which is then elongated by *cis*-undecaprenyl diphosphate synthase (UPPS) to *cis*-undecaprenyl diphosphate (UPP, **4**), the precursor of the lipid carrier undecaprenyl monophosphate (UP) used in peptidoglycan biosynthesis (Figure 1a). FPP is also elongated by long-chain *trans*-prenyl transferases to heptaprenyl diphosphate (HepPP, **5**), used in menaquinone-7 (MK-7, **6**) biosynthesis in *Staphylococcus aureus* (Figure 1a). In the mycobacteria, IPP and DMAPP form *cis*-FPP (**7**) which is

Received: July 4, 2020




https://dx.doi.org/10.1021/acsinfecdis.0c00472
ACS Infect. Dis. XXXX, XXX, XXX−XXX

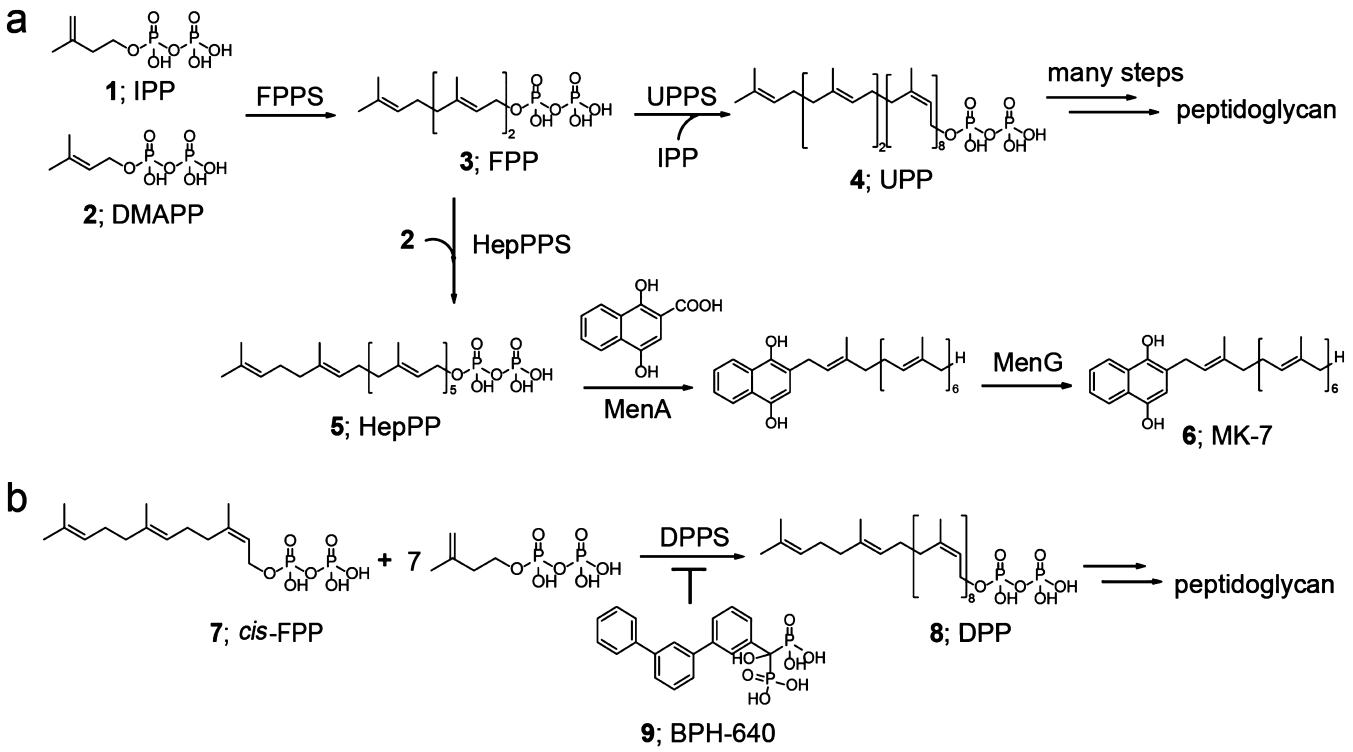


**Figure 1.** Schematic illustrations of some of the prenyltransferases, substrates, and products involved in peptidoglycan and quinone biosynthesis in bacteria. (a) Conversion of IPP (**1**) and DMAPP (**2**) to FPP (**3**) in most bacteria. The product is a *trans*-FPP and is converted by UPPS to UPP (**4**), on the route to cell wall biosynthesis, as well as to HepPP (**5**), catalyzed by a long-chain *trans*-prenyltransferase (here heptaprenyl diphosphate synthase), on the route to quinone (menaquinone (**6**) and/or ubiquinone) biosynthesis. (b) In mycobacteria, *cis*-FPP (**7**) is converted by a *cis*-decaprenyl diphosphate synthase (DPPS, Rv2361c in *Mycobacterium tuberculosis*) to *cis*-DPP (**8**), again on the route to cell wall biosynthesis. Also shown is a DPPS inhibitor, **9**.

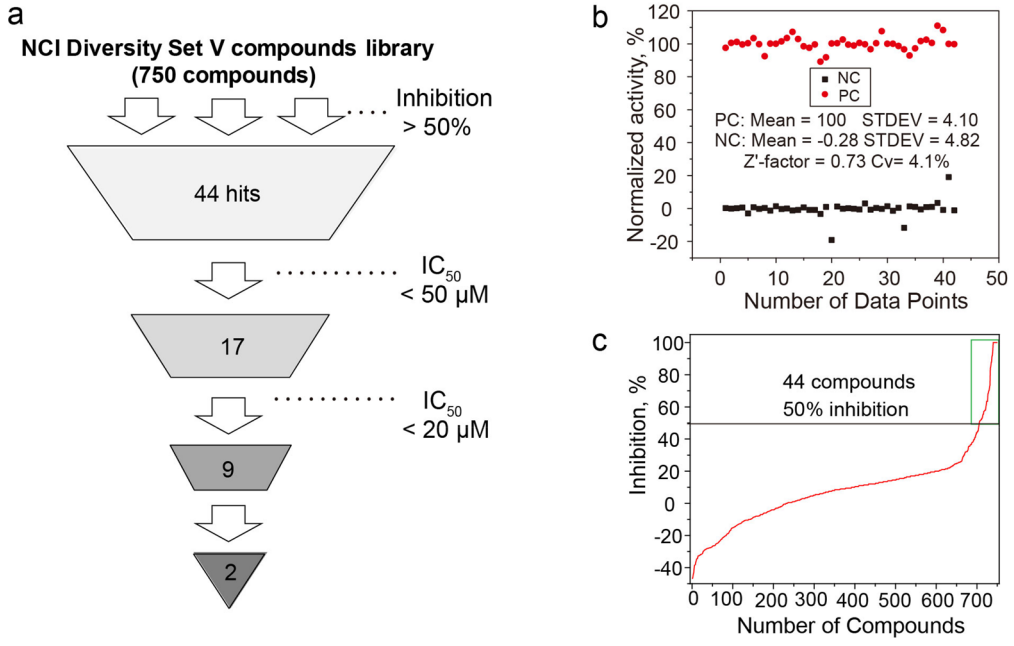


**Figure 2.** Screening results for MtDPPS inhibition using the 750-compound library. (a) Flowchart for MtDPPS inhibitor high-throughput screening and hit identification. (b) Results for quantify control of high-throughput screening showing a $Z'$ factor of 0.73. Enzymatic activities were normalized to the positive control (PC, with enzyme but no inhibitor added), after background subtraction with the negative control (NC, buffer only). Each data point represents the average value of positive or negative controls in one screening plate. (c) About 6% of the library compounds had $IC_{50}$ < 50 $\mu$M and were selected for dose−response assays. Some compounds exhibited a negative percentage of inhibition due to assay interference or the acceleration of the enzymatic reaction.


https://dx.doi.org/10.1021/acsinfecdis.0c00472
ACS Infect. Dis. XXXX, XXX, XXX−XXX

elongated to *cis*-decaprenyl diphosphate (DPP, **8**) by *cis*-decaprenyl diphosphate synthase (DPPS), also known as Rv2361c, in *Mycobacterium tuberculosis*.

The long-chain *cis*-prenyltransferases (*cis*-PTs) thus play an essential role in cell wall biosynthesis and are thought to be promising antibiotic targets since neither DPPS nor UPPS are made by humans. Plus, there is the possibility of synergistic effects with existing antibiotics that act in the same pathway.[3] There have been many screening campaigns directed at finding UPPS inhibitors,[4−7] albeit with limited success in cells (often due to plasma binding) or *in vivo*, and there have been no reports of screening campaigns against DPPS (from *M. tuberculosis*), although we did report the structure of a bisphosphonate inhibitor (BPH-640, **9**, $IC_{50}$ = 640 nM) bound to DPPS.[8]

Here, we screened a library of 750 compounds (from NCI Diversity Set 5) against *M. tuberculosis* DPPS (MtDPPS) finding several compounds with moderate ($IC_{50}$ = 5−10 $\mu$M) activity. Similar activity was also found with *Escherichia coli* UPPS (EcUPPS). These compounds were then tested for activity against a panel of pathogenic bacteria, and the most promising lead was then tested for *in vivo S. aureus*/*C. elegans* activity and for mammalian cell toxicity. We also carried out molecular docking investigations aimed at probing mechanisms of inhibitor binding, together with cell growth inhibition "rescue" experiments (with UP and a menaquinone) and testing for FPPS inhibition and uncoupling activity, in order to help elucidate the mechanisms of action of two lead compounds.

## RESULTS AND DISCUSSION

**Inhibitor Screening against MtDPPS.** MtDPPS was purified to >90% purity (Figure S1a), and its activity was monitored with a 2-amino-6-mercapto-7-methylpurine riboside (MESG) assay for phosphate release (Figure S1b,c). The screening flow-chart is shown in Figure 2a. Initial screening was performed using a 50 $\mu$M compound concentration, with **9** as the positive control. To assess the quality of the screen, we calculated the $Z'$ factor, which measures the ability of an assay to distinguish positive signals from the background.[9] A value of 1.0 represents an ideal assay, although a value of 0.7 is acceptable for high-throughput screening applications. We obtained a $Z'$ factor of 0.73 (Figure 2b), indicating adequate data quality for hit identification. Each data point in Figure 2b represents the average value of a positive or negative control in a screening plate. Figure 2c shows the rank-ordered percent MtDPPS inhibition in the presence of the screening library compounds.

Most compounds exhibited no or only very weak MtDPPS inhibition, <20% inhibition at 50 $\mu$M. However, 44 compounds were identified as having >50% inhibition, Figure 2c, and the $IC_{50}$ values for these compounds were then determined via dose−response curves. This hit rate is quite large and may be related to the DPPS ligand binding pocket also being large in order to accommodate polyisoprenoid substrates/intermediates. It is also known that UPPS[3] (as well as FPPS[10]) has allosteric sites, and allosteric site inhibitors are known for both; therefore, the "target promiscuity" (the high hit rate with DPPS; many diverse inhibitors for UPPS and FPPS) may be quite general for both *cis*- and *trans*-prenyltransferases. Out of 44 initial hits, 17 had $IC_{50}$ < 50 $\mu$M (Table 1), the best inhibition being by **10** (NSC73735, a.k.a. redoxal) which had an $IC_{50}$ value of 3.6 $\mu$M. Figures 3 and Figure S2 show the chemical structures of the more potent MtDPPS inhibitors (the most potent ones are in Figure 3). None of the compounds shown in Figure 3 or S2 were found to be Pan-assay interference compounds.[11] All compounds were also evaluated for their drug-likeness by analyzing their Lipinski parameters using the Molsoft server.[12] Drug-likeness scores are calculated by using a fragment-based approach with 5000 marketed drugs as a positive group and 10 000 nondrug compounds as the negative group. A score of −0.5 to 2 represents high drug-likeness, whereas values outside this range indicate the presence of non-drug-like features. The majority of the hits are thus drug-like except for **11**, **12**, **16**, and **24** (Table 1).

**Table 1. Rank-Ordered MtDPPS $IC_{50}$ Values, log *P*, Lowest p$K_a$, and Drug-Likeness Scores of the 17 Most Active MtDPPS Inhibitors**

| no. | NSC no. | MtDPPS $IC_{50}$, $\mu$M | log *P* | lowest p$K_a$ | drug likeness |
|---|---|---|---|---|---|
| **10** | NSC73735 | 3.6 | 5.95 | 3.52 | −0.2 |
| **11** | NSC159566 | 5.4 | 3.01 | 4.67 | −1.08 |
| **12** | NSC98363 | 5.9 | 3.81 | N.A. | −1.46 |
| **13** | NSC70931 | 8.9 | 6.56 | 4.78 | 0.63 |
| **14** | NSC227186 | 9.2 | 4.37 | 5.15 | 0.78 |
| **15** | NSC29200 | 11 | 4.39 | 12 | 0.32 |
| **16** | NSC345647 | 14 | 5.12 | 7.48 | −0.69 |
| **17** | NSC85433 | 17 | 5.62 | 5.11 | 0.88 |
| **18** | NSC127133 | 20 | 5.33 | 3.63 | −0.3 |
| **19** | NSC50688 | 23 | 4.55 | 7.7 | 0.08 |
| **20** | NSC60423 | 28 | 4.49 | 3.88 | 0.88 |
| **21** | NSC103331 | 33 | 4.18 | 10.23 | 0.51 |
| **22** | NSC215718 | 35 | 4.58 | 9.44 | 0.3 |
| **23** | NSC88600 | 37 | 4.02 | 15.26 | 0.02 |
| **24** | NSC97920 | 37 | 5.36 | N.A. | −1.3 |
| **25** | NSC50651 | 40 | 4.77 | 7.64 | 0.63 |
| **26** | NSC176736 | 46 | 5.45 | 14.44 | 0.05 |

**Inhibition of Other Prenyltransferases.** The 17 initial hits with $IC_{50}$ < 50 $\mu$M (Figures 3 and S2) obviously exhibit very broad structural diversity, but several share some common features. First, most are relatively hydrophobic with log *P* values ranging from ∼3 to ∼6.6 (Table 1), as calculated by the Pan-assay interference compounds remover,[11] which presumably enables them to mimic the hydrophobic polyisoprenyl group of the MtDPPS substrate, *cis*-FPP. Second, 6 of the 9 more potent inhibitors have $IC_{50}$ values of <20 $\mu$M and are predicted to have a p$K_a$ of <5.5 (Table 1), calculated by using the Molsoft server,[12] but only 1 out of 8 compounds in the less active group have a p$K_a$ of <5.5. This suggests that an anionic group is a desirable feature of MtDPPS inhibition. Third, except for **14**, anionic groups are located at the ends of the molecule. Most active compounds thus share a "polar-hydrophobic" scaffold that mimics the structure of one of the substrates, *cis*-FPP. The results of quantum chemical (density functional theory, DFT) calculations support this polar-hydrophobic picture, as shown in the molecular electrostatic potential surfaces in Figure S3. Given the general structural similarity between *cis*- and *trans*-FPP, we hypothesized that some of the DPPS inhibitors might also inhibit UPPS, which uses *trans*-FPP as one substrate as well as *trans*-FPPS, which has an allosteric FPP binding site.[13] We found that the most potent MtDPPS inhibitor, redoxal (**10**), inhibited a bacterial UPPS (EcUPPS) with $IC_{50}$ = 7.8 ± 3.3


https://dx.doi.org/10.1021/acsinfecdis.0c00472
ACS Infect. Dis. XXXX, XXX, XXX−XXX

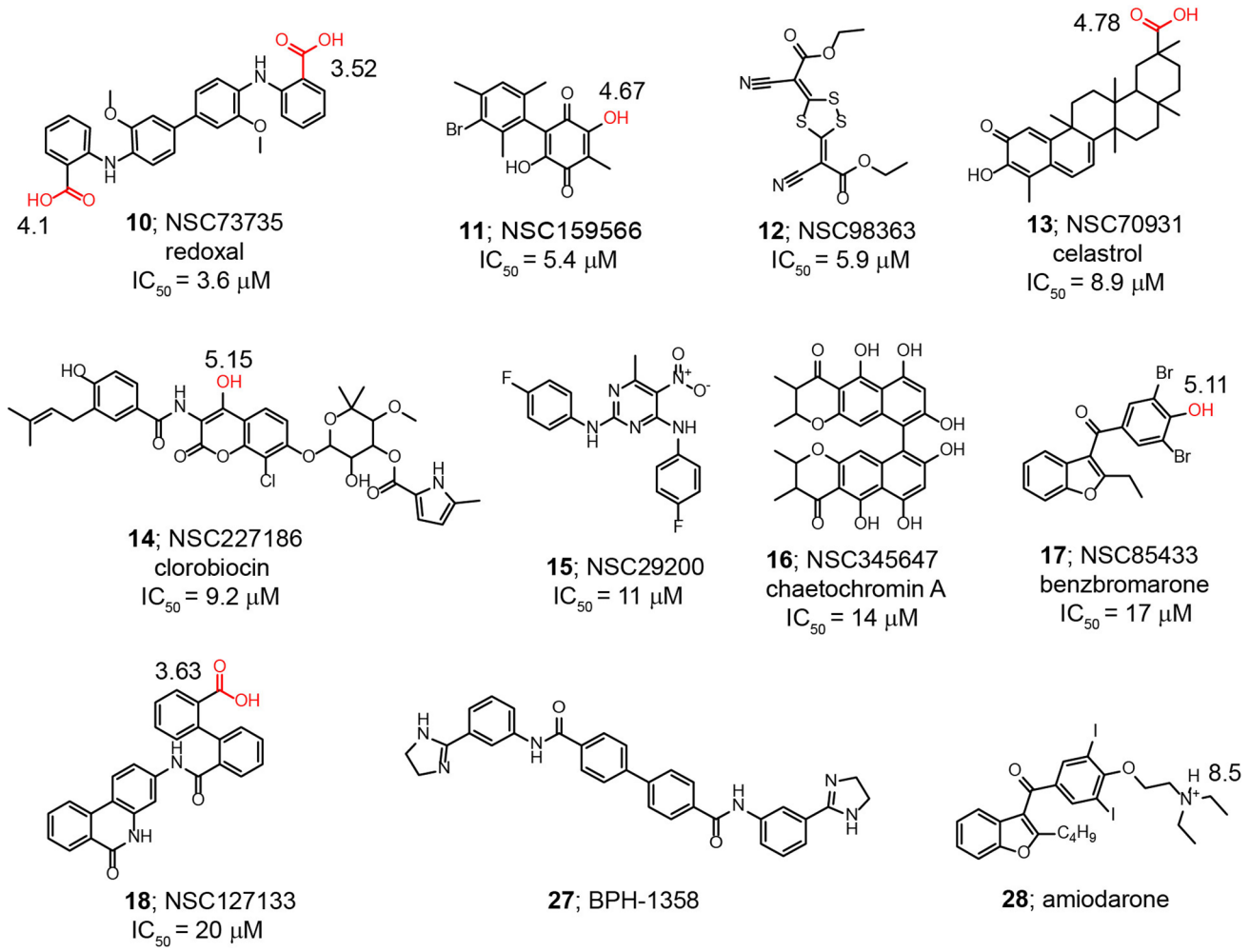


**Figure 3.** Chemical structures of MtDPPS inhibitors with $IC_{50}$ values below 20 $\mu$M, as well as other compounds of interest.

$\mu$M (Figure S4a). The $IC_{50}$ 95% confidence interval was 5.9–11 $\mu$M as determined by a four-parameter variable slope function with $R^2$ = 0.88 using 24 data points. The Hill slope was 3 (SE = 1), which may indicate some effects of aggregation or perhaps, binding at more than one site. Moreover, we found that redoxal inhibited an ortholog of bacterial FPPS, human FPPS (HsFPPS), with $IC_{50}$ = 3.4 ± 0.43 $\mu$M (Figure S4b). The $IC_{50}$ 95% confidence interval was 2.8–4.9 $\mu$M as determined by a four-parameter variable-slope function with $R^2$ = 0.99 with 12 data points. The Hill slope was 2 (SE = 0.35), which again may indicate some effects of aggregation or perhaps binding at more than one site. Interestingly, in previous work[14] we found that the bisamidine inhibitor of UPPS, BPH-1358 (Figure 3, **27**) was also an FPPS inhibitor and **10** and **27** share a common structural feature—a biphenyl core. Thus, **10** can inhibit both DPPS and UPPS as well as FPPS. The following questions then arise: How might **10** bind to DPPS, UPPS, and FPPS? Does **10** have antibacterial activity? Is it toxic to mammalian cell lines? Does it have activity *in vivo*, in an animal model (*S. aureus*/*C. elegans*) system?

**Mechanisms of Prenyltransferase Inhibition.** In order to see how redoxal (**10**) might inhibit all three enzymes, we next used molecular docking using the X-ray structures of MtDPPS (PDB ID code 2VG3), EcUPPS (PDB ID code 1X06), *S. aureus* UPPS (PDB ID code 4H8E), and HsFPPS (PDB ID code 5JA0). We show in Figure 4a–c docking results for **10** binding to MtDPPS, SaUPPS, and HsFPPS. Results for EcUPPS are very similar to those for SaUPPS and are shown in Figure S5a. Protein backbones are shown as gray cartoons, amino acid residues are gray sticks, **10** is shown in magenta stick form, and substrate-like ligands are shown as yellow sticks. Figures 4d–f and S5b show aligned structures of **10** with the GPP substrate-analog citronellyl (dihydrogeranyl) diphosphate (yellow) bound to MtDPPS (Figure 4d), FPP bound to SaUPPS (Figure 4e), FPP bound to EcUPPS (Figure S5b), and FPP bound to HsFPPS (Figure 4f). The electrostatic potential surfaces (ESPs) in the ligand binding sites are shown in Figures 4a–c and S5a in which blue = positive, white = neutral, and red = negative regions.

The ESP surface results show that there is an electropositive region at the "top" of the *cis*-PT structures, DPPS (Figure 4a) and UPPS (Figures 4b and S5a), which arises from the presence of $Mg^{2+}$ and a cluster of Arg residues. **10** binds to this region with one of its carboxylates interacting with the $Mg^{2+}$ and an Arg residue, while the hydrophobic part of the molecule occupies a tunnel, surrounded by hydrophobic residues, as shown in the ligand-interaction plots in Figure S6a–c. Compound **10** has essentially the same length as does the (initial) FPP substrate for these enzymes and so can readily bind into this hydrophobic cavity. However, in the case of the *trans*-prenyltransferase (*trans*-PT) FPPS, FPP is a product of


https://dx.doi.org/10.1021/acsinfecdis.0c00472
ACS Infect. Dis. XXXX, XXX, XXX–XXX

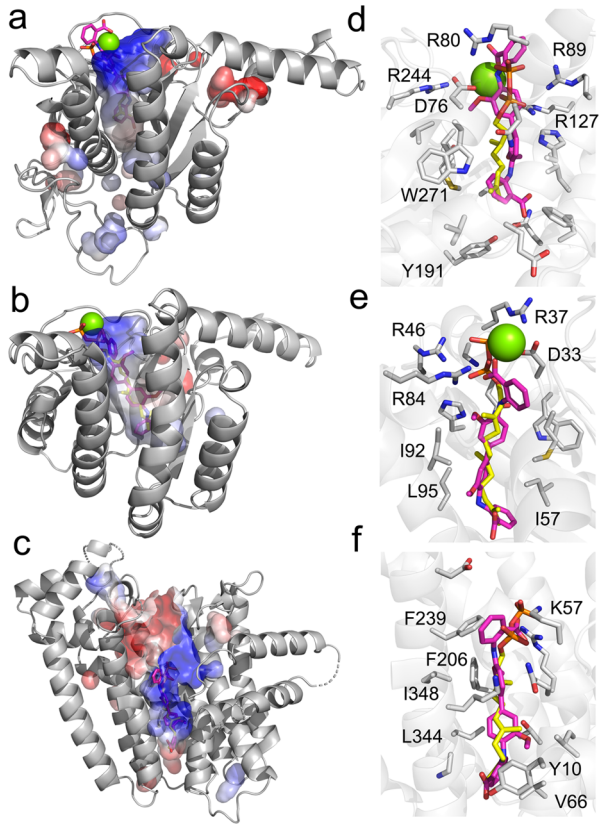


**Figure 4.** Structures of MtDPPS, SaUPPS, and HsFPPS with docked **10**. For each panel shown on the left, protein backbones are shown as gray cartoons, and the electrostatic potential surfaces (EPSs) of the active sites as calculated with Pymol are shown, with blue indicating a positively charged surface, white indicating a neutral surface, and red indicating a negatively charged surface. (Right) Close-up views of **10** (in magenta) docked into the active sites showing residues of interest (as gray sticks) together with the substrates or inhibitors (in yellow) from the crystal structures. (a) MtDPPS with bound citronellyl diphosphate, PDB ID code 2VG3. (b) SaUPPS with bound FPP, PDB ID code 4H8E. (c) HsFPPS bound with FPP, PDB ID code 5JA0. (d) Close-up view of (a). (e) Close-up view of (b). (f) Close-up view of (c). Full protein–ligand interactions are shown in Figure S6.

this enzyme and does not bind to the allylic binding site but rather binds to an allosteric or regulatory site, and there is no $Mg^{2+}$ present in the structure.[13] The ESP surface result (Figure 4c) now shows that the "top" of the structure is electronegative since there are six Asp residues present that normally bind to 3 $Mg^{2+}$ during catalysis. The results of the docking calculations indicate that **10** binds to the same allosteric site as does FPP (Figure 4f) and binding is due primarily to hydrophobic interactions (Figure S6d). The FPPS structure is an open one and can accommodate large ligands, as reported, for example, with diterpenoid inhibitors.[15] While it is not certain whether such an allosteric site is present in bacterial FPPSs, there is close similarity between the three-dimensional structures of human and bacterial FPPS [e.g., a 2.66 Å C$\alpha$ rmsd over 156 residues between HsFPPS and SaFPPS (PDB ID codes 5JA0 and 1RTR) and a 2.49 Å C$\alpha$ rmsd over 177 residues between HsFPPS and EcFPPS (PDB ID codes 5JA0 and 1RQI)]. Moreover, the observation that **10** has activity against HsFPPS is of interest in the context of whether it might be toxic to human cells.

Taken together, the docking results indicate that electrostatic/H-bond interactions are likely to be important for the binding of **10** to the *cis*-PTs DPPS and UPPS. However, given the small number of active compounds in the MtDPPS assays together with the small range in $IC_{50}$ values, it is not possible to use quantitative structure–activity models to make accurate predictions of activity.[16] Nevertheless, it is of interest to note that when we computed 365 descriptors in the MOE program,[17] the two descriptors that gave the best correlations with MtDPPS activity were H-bond or hydrophilic descriptors (vsurf_HB2 and vsurf_CW4), with Pearson correlation coefficients of $R$ = 0.74–0.76, as shown in Figure S7, consistent with the observation of electrostatic/H-bond interactions in the docking results. The question then arises as to whether **10** (and other compounds) have activity in cells and *in vivo*.

**Antimicrobial Activity.** We next tested the nine most potent MtDPPS inhibitors (**10**–**18**, Figure 3) against the following panel of Gram-negative and Gram-positive bacteria: *Mycobacterium smegmatis*, *Klebsiella pneumoniae*, *Acinetobacter baumannii*, *Pseudomonas aeruginosa*, *S. aureus*, and *Clostridioides difficile*. As shown in Table 2, although there was a general lack of activity against *M. smegmatis* and the Gram-negative bacteria (*K. pneumoniae*, *A. baumannii*, and *P. aeruginosa*), several compounds displayed moderate to potent activity against Gram-positive pathogens (*S. aureus* and *C. difficile*). Compound **14** was the only broad-spectrum antibacterial with MIC values ranging from <0.05 to 33 $\mu$M against the tested pathogens. However, compound **14** is actually the antimicrobial clorobiocin that inhibits DNA gyrase,[18] but here we found that clorobiocin also inhibits MtDPPS (with an $IC_{50}$ of 9.2 $\mu$M), suggesting that *cis*-PT inhibition may be a

**Table 2. Antimicrobial Activity of the Top Nine MtDPPS Inhibitors**[a]

| | | | MIC, $\mu$M | | | |
|---|---|---|---|---|---|---|
| no. | NSC no. | MtDPPS $IC_{50}$, $\mu$M | *M. smegmatis* | Gram-negative pathogens | *S. aureus* | *C. difficile* |
| 10 | NSC73735 | 3.6 | >100 | >100 | 11 | 4 |
| 11 | NSC 159566 | 5.4 | >100 | >100 | 11 | 16 |
| 12 | NSC98363 | 5.9 | 33 | >100 | 33 | 64 |
| 13 | NSC70931 | 8.9 | >100 | >100 | 0.41 | 1 |
| 14 | NSC227186 | 9.2 | 33 | 1.2–11 | <0.050 | <0.50 |
| 15 | NSC29200 | 11 | >100 | >100 | >100 | >64 |
| 16 | NSC345647 | 14 | >100 | >100 | 0.41 | <0.50 |
| 17 | NSC85433 | 17 | >100 | >100 | 11 | 4 |
| 18 | NSC127133 | 20 | >100 | >100 | >100 | >64 |

[a]**14** was also active against the three Gram-negative pathogens (*K. pneumoniae*, 11 $\mu$M; *A. baumannii*, 1.2 $\mu$M; and *P. aeruginosa*, 11 $\mu$M).


https://dx.doi.org/10.1021/acsinfecdis.0c00472
ACS Infect. Dis. XXXX, XXX, XXX–XXX

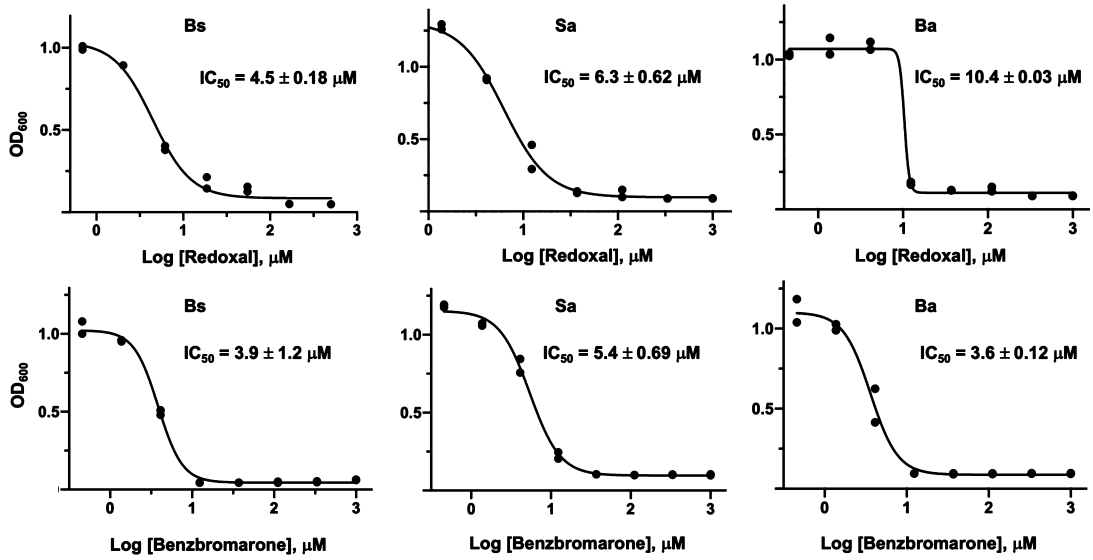


**Figure 5.** Dose−response curves for redoxal (**10**) and benzbromarone (**17**) inhibition of the growth of *B. subtilis* (Bs), *S. aureus* (Sa), and *B. anthracis* Sterne (Ba). (Top) Growth inhibition by redoxal. (Bottom) Growth inhibition by benzbromarone. Results shown are representative duplicates from ≥3 sets of experiments.

secondary target. Several other MtDPPS inhibitors also possess moderate to potent inhibitory activity against Gram-positive bacteria *S. aureus* and *C. difficile* (Table 2), with **13** and **16** being very potent. Compound **13**, also known as celastrol, has been of interest in the context of the development of therapeutics to treat a wide range of diseases,[19,20] and previously we found that it also inhibits a polyisoprenyl transferase, squalene synthase, from *Aspergillus flavus*.[21] However, since celastrol can react with proteins via Michael addition,[22] it is not a desirable *cis*-PT inhibitor. Compound **16** (a.k.a. chaetochromin A) also has a broad range of biological activities,[23,24] including antimicrobial activity, but deducing the mechanism of its antimicrobial activity has been elusive. Here, we find that *cis*-PT inhibition is one possible target, but since chaetochromin A exhibits high *in vivo* toxicity,[25] its development as an antimicrobial seems unlikely, consistent with our drug-likeness predictions.

Compounds **10** (redoxal), **11**, and **17** (a.k.a. benzbromarone) are all moderately active against *S. aureus* and *C. difficile*. Compound **11** was not previously reported to have any bioactivity and it has a non-drug-like structure, so **11** is not likely to be a productive hit or lead as a *cis*-PT inhibitor. On the other hand, the best MtDPPS inhibitor, **10**, was reported to inhibit dihydroorotate dehydrogenase[26] and ribonucleotide reductase[27] (although the purity was not specified, and samples we obtained from Sigma and the NCI were only ∼65% pure) and also inhibits MtDPPS, UPPS, and FPPS as well as Gram-positive bacterial cell growth with the following $IC_{50}$ (from four-parameter fits) or MIC values: *S. aureus* 6.3 ± 0.62 μM, *C. difficile* 4.0 μM, and *Bacillus anthracis* Sterne 10.4 ± 0.03 μM as well as model system *B. subtilis* 4.5 ± 0.18 μM (Figure 5a and Table 2). Therefore, it appeared to be of interest for the mechanism of action studies. We also found that **10** was active against several *S. aureus* clinical strains (Table S1) and investigated possible synergistic interactions of **10** with 174 FDA-approved antibiotics against *S. aureus* Newman. At half of the MIC of **10**, we found that some antibiotics, especially aminoglycosides and β-lactams (Figure S8 and Table S2), exhibited significant synergy (Table S2).

We also found that **17**, an FDA-approved uricosuric agent used in the treatment of gout,[28] is a *cis*-PT inhibitor (MtDPPS $IC_{50}$ 17 μM) and also a bacterial cell growth inhibitor ($IC_{50}$ or MIC values: *S. aureus* 5.4 ± 0.69 μM, *C. difficile* 4.0 μM, *B. subtilis* 3.9 ± 1.2 μM, and *B. anthracis* Sterne 3.6 ± 0.12 μM; Figure 5b and Table 2). Benzbromarone was previously reported to have antimicrobial activity against *S. aureus*,[29] and it has synergistic effects with minocycline in the inhibition of *S. aureus*.[30] It also exhibits antivirulence activity including disrupting quorum sensing, preventing biofilm formation, and inhibiting staphyloxanthin pigment biosynthesis.[29,31] Therefore, both **10** and **17** appeared to be of interest as potential multitargeting antimicrobials. The bacterial growth inhibition of **10** and **17** against the Gram-positive pathogens tested also suggested that they might inhibit Gram-negative bacteria in the presence of the Gram-negative bacteria sensitizer pentamidine,[32] and we found that pentamidine potentiates the effects of **10** and **17** in *A. baumannii* growth inhibition, resulting in a >400-fold reduction in MIC with **17** (Figure S9).

**Cell Growth Inhibition Rescue Experiments.** Since both **10** and **17** have activity against several Gram-positive bacteria, the question then arises as to whether this activity is against UPPS and/or FPPS (both found in both Gram-positive and Gram-negative bacteria) or if other mechanisms are involved. We thus next sought to determine to what extent we could "rescue" bacterial cell growth inhibition by adding a (putative) end product whose biosynthesis might be inhibited by **10** or **17**. If FPPS/UPPS inhibition is significant, then it should be possible to rescue cells (i.e., to increase the $IC_{50}$ for cell growth inhibition) by adding a downstream product such as UP, formed from UPP by undecaprenyl diphosphate phosphatase. If the growth inhibition was primarily due to FPP inhibition, then it should be possible to rescue cell growth by the addition of a quinone (e.g., MK-4) plus UP, an approach we have used recently with bisphosphonate inhibitors.[33] As can be seen in Figure 6a,b, the addition of UP (at 50 μM) resulted in a 3.4-fold increase in the $IC_{50}$ for *B. subtilis* cell growth inhibition (from 4.5 to 15.5 μM), while the addition of MK-4 (menaquinone with a $C_{20}$ side chain, a


https://dx.doi.org/10.1021/acsinfecdis.0c00472
ACS Infect. Dis. XXXX, XXX, XXX−XXX

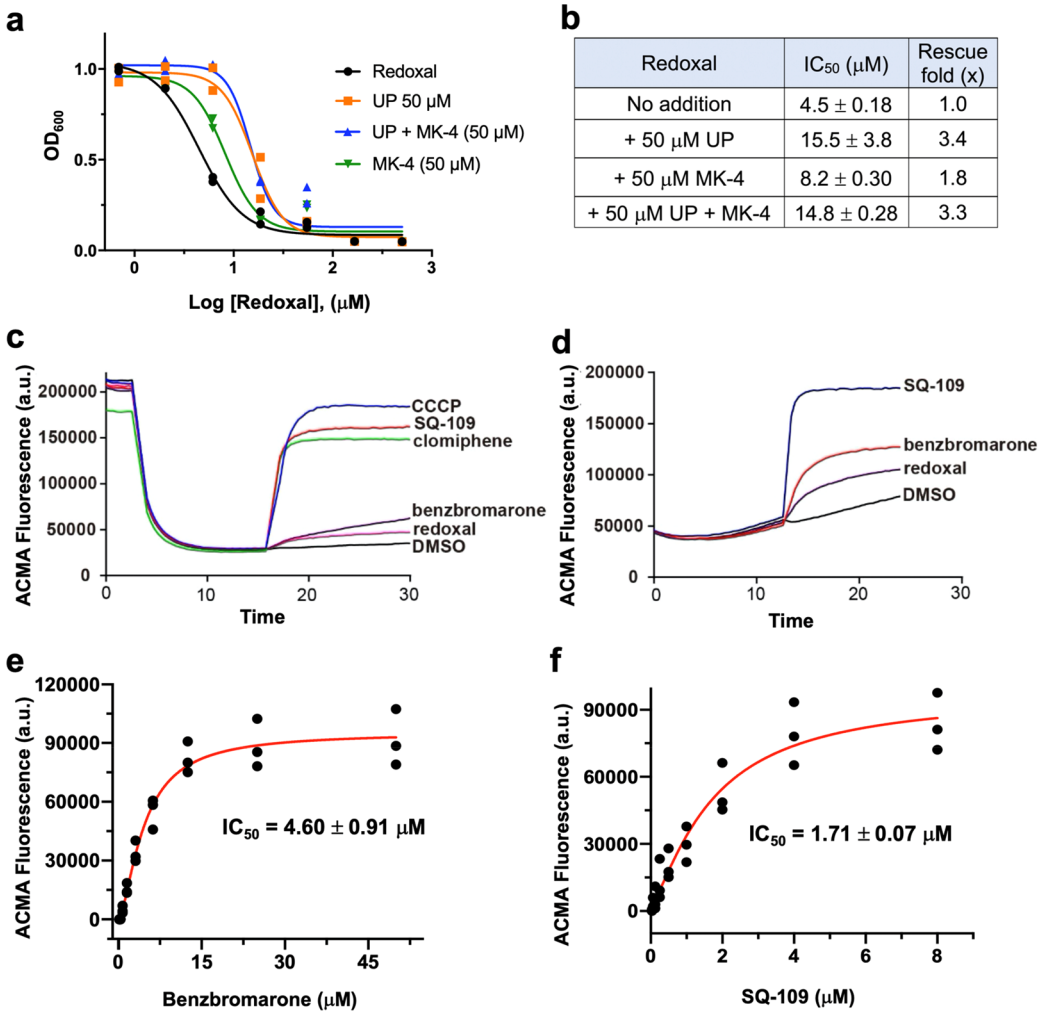


| Redoxal | $IC_{50}$ (μM) | Rescue fold (x) |
|---|---|---|
| No addition | 4.5 ± 0.18 | 1.0 |
| + 50 μM UP | 15.5 ± 3.8 | 3.4 |
| + 50 μM MK-4 | 8.2 ± 0.30 | 1.8 |
| + 50 μM UP + MK-4 | 14.8 ± 0.28 | 3.3 |

**Figure 6.** Mechanism of action results showing the effects of undecaprenyl phosphate (UP) and menaquinone-4 (MK-4) on *B. subtilis* growth inhibition by redoxal, together with uncoupler results for redoxal, benzbromarone, and other known uncouplers (CCCP, clomiphene, and SQ-109). (a) Dose−response curve for *B. subtilis* growth inhibition "rescue" effects caused by UP (50 $\mu$M, orange squares), MK-4 (50 $\mu$M, green triangles), or UP+MK-4 at 50 $\mu$M each (blue triangles). The redoxal-control results are shown as black circles. (b) $IC_{50}$ values for *B. subtilis* growth inhibition together with "rescue effects" and the $IC_{50}$ *x*-fold increase on addition of the rescue agent. Experiments were performed in duplicate. (c−f) Effects of known protonophore uncouplers, redoxal (**10**) and bromobenzarone (**17**), on ACMA fluorescence in *E. coli* IMVs. (c) Effects of SQ-109, clomiphene, carbonyl cyanide *m*-chlorophenyl hydrazine (CCCP), redoxal (**10**), and benzbromarone (**17**) on ACMA fluorescence using ATP hydrolysis to drive ΔpH. (d) The same as for (c) but with succinate-generated ΔpH. (e) Dose−response curve for ATP-powered ΔpH collapse with benzbromarone (**17**); $IC_{50}$ = 4.6 ± 0.91 $\mu$M. (f) The same as for (e) but with SQ-109; $IC_{50}$ = 1.7 ± 0.07 $\mu$M.

geranylgeranyl group) resulted in a 1.8-fold increase. The addition of UP+MK-4 did not improve the rescue effect, consistent with an additional effect that limited the extent of the rescue. With benzbromarone, there were no effects of UP, MK-4, or UP+MK-4 addition, indicating a non-UPPS or FPPS mechanism of action in bacterial growth inhibition, consistent with the lack of inhibition of UPPS or FPPS (data not shown).

**Protonophore Uncoupler Activity.** Both redoxal and benzbromarone are lipophilic species that contain ionizable groups, and on the basis of previous work,[34] it appeared possible that both compounds might act, at least in part, as protonophore uncouplers, collapsing the proton motive force (PMF) in bacteria, a known effect of benzbromarone in mitochondria. We therefore next tested redoxal and benzbromarone in an *E. coli* inverted membrane vesicle (IMV) assay in which either succinate or ATP is used to drive $H^+$ (through the ATPase) into the membrane interior, resulting in self-aggregation of the 9-amino-6-chloro-2-methoxyacridine (ACMA) fluorophore.[34] The addition of either redoxal or benzbromarone (at 1 $\mu$M) resulted in the $H^+$ efflux/pH gradient collapse and reversed ACMA quenching, as shown in Figure 6c,d. We used protonophore SQ-109 as a control, finding that benzbromarone is a more potent protonophore uncoupler than redoxal but is less effective than SQ-109, a lipophilic amine. The differences between the succinate and ATP results are due to differences in the rates of $H^+$ influx. These results show, therefore, that redoxal is a weak uncoupler while benzbromarone is more potent. The computed $pK_a$ values for redoxal are 3.5 and 4.1; log *P* is 8.1, and log $D_{7.4}$ (log *P* at pH 7.4, calculated by using the Molsoft server)[31] is 1.6. For benzbromarone, the computed $pK_a$ is 5.1, log *P* is 5.62, and log $D_{7.4}$ is 3.69. Thus, at pH 7.4, it appears likely that there will be more benzbromarone in cell membranes than would be found with redoxal, resulting in better uncoupling activity, as previously observed.[35] As can be seen in Figure 6e,f, the $IC_{50}$ value for uncoupling activity with


https://dx.doi.org/10.1021/acsinfecdis.0c00472
ACS Infect. Dis. XXXX, XXX, XXX−XXX

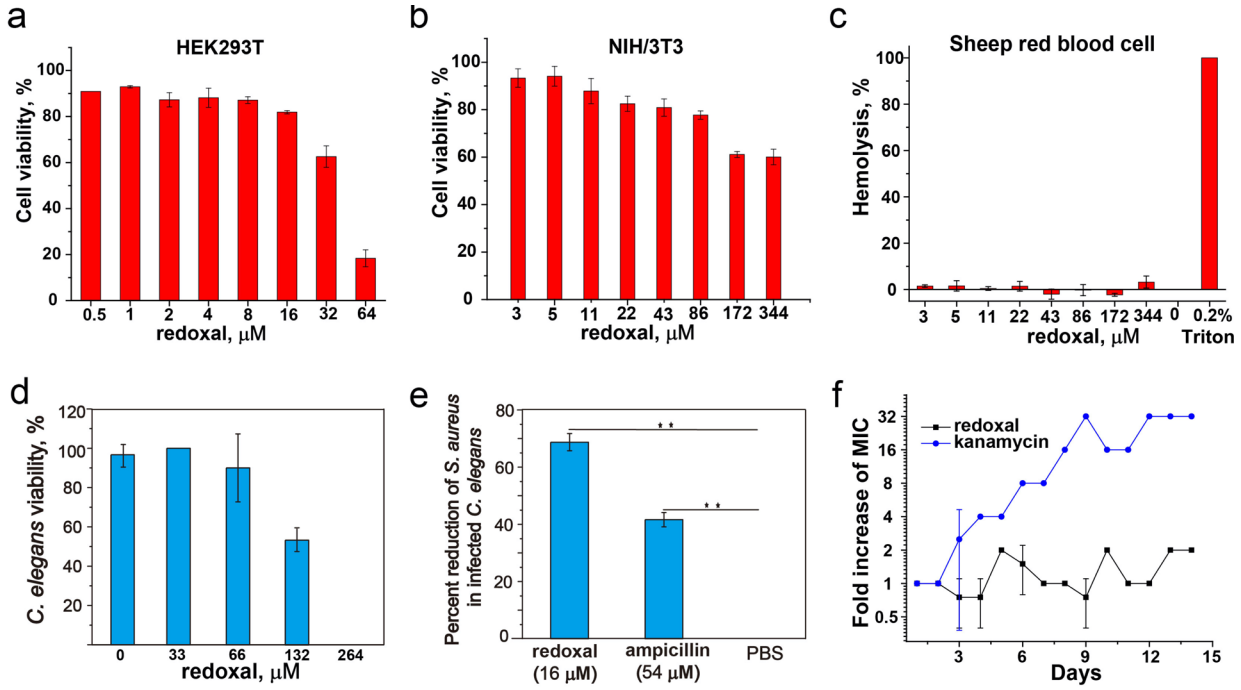


**Figure 7.** Effects of redoxal (**10**) on mammalian cell growth, *C. elegans* viability, and *S. aureus* growth in *C. elegans*. (a, b) Cytotoxicity assay using the HEK293T and NIH/3T3 cell lines; data from 3 sets of experiments. (c) Hemolytic toxicity assay using sheep red blood cells. (d) Survival rate of *C. elegans* treated with **10**. (e) *In vivo* antimicrobial activity of **10** (16 $\mu$M), ampicillin (54 $\mu$M) or PBS (control) on the percentage reduction of *S. aureus* in *C. elegans*. Data analyzed using student's *t* test, and significant differences between groups are marked with an asterisk (**$P < 0.01$). Experiments were repeated three times. (f) Resistance development comparison between **10** and kanamycin against *S. aureus* Newman.

benzbromarone is 4.6 ± 0.91 $\mu$M, about twice that of SQ-109, a more potent ($IC_{50}$ = 1.7 ± 0.07 $\mu$M) protonophore uncoupler that targets MmpL3[36] and is in clinical trials for tuberculosis.

From a structural perspective, it is also interesting that the FDA-approved class III antiarrhythmia drug amiodarone (**28**) has the same benzofuran core structure as does benzbromarone but the side chains are different. In the case of amiodarone, the side chain contains a diethylaminoethyl group which has a $pK_a$ of ∼8.5, while in benzbromarone, the dibromophenol group is expected to have a $pK_a$ of ∼5.1. Thus, in both amiodarone and benzbromarone, protons can be shuttled across membranes, collapsing the pH gradient. In fact, in previous work[37] it was proposed that the optimum $pK_a$ for uncouplers was ∼7.2 with a log *P* of ∼5.5, and there is a V-shaped dependence of uncoupling activity on $pK_a$. Benzbromarone is thus on one side of the curve ($pK_a \approx 5.5$) that has a minimum at pH ≈ 7.2 while amiodarone ($pK_a \approx 8.5$) is on the other side of the curve.

In summary, the results of the UPPS, DPPS, and FPPS inhibition assays, the protonophore uncoupling assays in inverted membrane vesicles, and the cell growth inhibition assays all point to a combined isoprenoid biosynthesis inhibition plus a mild uncoupling mechanism for redoxal, while with benzbromarone, uncoupling appears to be an important target presumably contributing to its previously reported activity against *S. aureus*.[29]

***In Vivo* Activity and Toxicity of 10.** Finally, we investigated the potential toxicity and *in vivo* activity of **10**. For cytotoxicity, we used a human embryonic kidney cell line (HEK293T) and mouse embryonic fibroblasts (NIH/3T3); sheep red blood cells were used for hemolytic toxicity testing, while for *in vivo* activity we used the *S. aureus*/*C. elegans* model. In the HEK293T and NIH/3T3 assays, the result showed a low cytotoxicity of **10** (Figure 7a,b), and the $IC_{50}$ values for cell growth inhibition were 54 $\mu$M (95% CI 46−66 $\mu$M) and 240 $\mu$M (95% CI 210−270 $\mu$M) (Figure S10). The hemolysis assay indicated that **10** had no obvious hemolytic toxicity until >300 $\mu$M (Figure 7c). Results for *C. elegans* viability are shown in Figure 7d, in which it can be seen that redoxal (**10**) has low toxicity ($LD_{50}$ = 89 $\mu$M, Figure S11). Efficacy, expressed as the percent reduction in *S. aureus* survival in *C. elegans*, is shown in Figure 7e. As shown in Figure 7e, there is an ∼70% reduction in *S. aureus* viability at 16 $\mu$M redoxal (**10**), a concentration at which there is no effect on *C. elegans* viability or on mammalian cell growth. Plus, there is clearly more activity than is found with ampicillin (at 54 $\mu$M). In addition, in a comparison with kanamycin, there was no increase in the MIC of **10** after 14 daily passages while there was a 32-fold increase in the MIC of kanamycin (Figure 7f).

## CONCLUSIONS

Inhibition of the *cis*-PTs DPPS and UPPS is a potentially important route to the development of new antimicrobial agents. Here, we tested 750 compounds to identify inhibitors of MtDPPS and obtained 17 compounds with $IC_{50}$ values ranging from 3.6 to 46 $\mu$M. We tested the more active compounds for antimicrobial activity against *M. smegmatis*, *K. pneumoniae*, *A. baumannii*, *P. aeruginosa*, *S. aureus*, and *C. difficile*, finding that several compounds had moderate to potent activity. Redoxal (**10**) and benzbromarone (**17**) were identified as the most promising hits and were also found to be active against *B. anthracis* Sterne and *B. subtilis*. We also found that **10** was an inhibitor of UPPS as well as FPPS and a weak protonophore uncoupler. Computational docking indicated that **10** binds to the DPPS and UPPS allylic binding sites via


https://dx.doi.org/10.1021/acsinfecdis.0c00472
ACS Infect. Dis. XXXX, XXX, XXX−XXX

$Mg^{2+}$ and Arg but to the FPP allosteric site in FPPS. **17** had no activity against UPPS or FPPS but was a more potent protonophore uncoupler, consistent with computed p$K_a$, log *P* and log $D_{7.4}$ values. *B. subtilis* cell growth inhibition by **10** was rescued by UP (3.4-fold) but less so by MK-4, consistent with an additional target, the proton motive force (PMF). We also found a relatively low toxicity of **10** against human (HEK293T) and mouse (NIH/3T3) cell lines, low hemolytic activity, and promising *in vivo* activity in an *S. aureus*/*C. elegans* infection model. In the future, it will clearly be of interest to obtain structures of **10** bound to DPPS, UPPS, and FPPS and to develop analogs in order to obtain more potent multitarget leads. It is now becoming clear[34] that several antibacterials, such as bedaquiline, clofazimine, and SQ-109, target both enzymes and the proton motive force, as here with **10**. Of course, caution must be exercised in the use of compounds with uncoupling activity, especially if taken for long periods (such as with the *M. tuberculosis* drugs or amiodarone), but for shorter periods of use, combining the effects of targeting bacterial prenyltransferases with the PMF may be an attractive possibility.

## METHODS

**Chemicals.** 2-Amino-6-mercapto-7-methylpurine riboside (MESG) and purine nucleoside phosphorylase (PNP) were purchased from ThermoFisher, and inorganic pyrophosphatase (PPase), redoxal, 9-amino-6-chloro-9-amino-6-chloro-2-methoxyacridine (ACMA), clomiphene, *m*-chlorophenylcarbonyl cyanide phenylhydrazone (CCCP), succinate, adenosine triphosphate (ATP), MOPS−KOH, HEPES−KOH, KCl, and menaquinone-4 (MK-4) were from Sigma-Aldrich. $MgCl_2$ was from Merck. Benzbromarone was purchased from Carbosynth, product no. FD18180. Compound **9** (BPH-640) was synthesized as reported previously.[8] Undecaprenyl monophosphate (UP) was from Larodan AB, Sweden (product no. 62-1055-2). Ampicillin and 3-(4,5-dimethylthiazol-2-yl)-2,5-diphenyltetrazolium bromide (MTT) were purchased from Hefei Bomei Biotechnology Co., Ltd.

**Cells.** Bacteria were kindly provided by Professor Douglas A. Mitchell and were as follows: *B. subtilis* from subsp. *subtilis* (Ehrenberg) Cohn ATCC 6051; *E. coli* (K12, ATCC 29425); *E. coli* (BL21 (DE3), New England Biolabs); *S. aureus* Newman strain (ATCC 25904); *M. smegmatis* (MC2 155, ATCC 700084); *B. anthracis* (str. Sterne); *C. difficile* (ATCC 43255); *A. baumannii* (Bouvet and Grimont, ATCC 19606); and *K. pneumoniae* (subsp. *pneumoniae* Schroeter Trevisan ATCC 27736). *P. aeruginosa* PA01, *S. aureus* clinical strains 1−5, and USA 300 were from Professor Zhi Su. All bacterial strains were confirmed by 16S DNA sequencing. The human embryonic kidney cell line (HEK293T, ATCC CRL-3216) and mouse embryonic fibroblast cells (NIH/3T3, ATCC CRL-1658) were purchased from the American Type Culture Collection (ATCC, Manassas, VA). *C. elegans* (N2) was acquired from the *Caenorhabditis* Genetics Center.

**Purification of Redoxal.** Redoxal (**10**) came with a warning that purity was not guaranteed, and indeed qNMR yielded only 65% purity. We thus carried out a purification using lixiviation. Redoxal (200 mg) was stirred with 10 mL of MeOH/$Et_2O$ (3:1, v/v) for 10 h at 40 °C under a $N_2$ atmosphere, the supernatant was then discarded, and the solid was re-extracted twice to yield a solid which after drying *in vacuo* was found to be 95% pure by qNMR (using 1,3,5-trimethoxybenzene as an internal standard and a 5 mm cryprobe on a 500 MHz Bruker NMR instrument) (Figure S12). Benzbromarone (**17**) was ∼98% pure by qNMR (using Mnova software) (Figure S13).

**MtDPPS Cloning, Expression, and Purification.** MtDPPS was prepared as previously reported.[8] In brief, the gene encoding *cis*-decaprenyl diphosphate synthase (DPPS; Rv2361c) from *M. tuberculosis* was cloned into the pET28a vector, and then the plasmids were transformed to *E. coli* BL21 (DE3) and cultured in tryptone-phosphate medium at 37 °C until the $OD_{600}$ reached 0.7−0.8. Protein expression was induced with 1 mM isopropyl-*β*-D-thiogalactopyranoside (IPTG) at 20 °C for 24 h. Cells were then lysed by sonication, and debris was removed by centrifugation. The resulting supernatant was then loaded onto a Ni-NTA column equilibrated in buffer containing 50 mM phosphate (pH 7.2), 300 mM NaCl, and 30 mM imidazole. His-tagged Rv2361c was eluted using an imidazole gradient (20−250 mM).

**Enzyme Inhibition Assays: General Methods.** Enzyme inhibition was determined with a continuous spectrophotometric assay for inorganic phosphate release using the substrate MESG and the enzyme PNP.[38] For the prenyltransferase assays, Ppase was added to the reaction mixture to convert each pyrophosphate to two inorganic phosphates. The inorganic phosphate then reacts with MESG in a PNP-catalyzed reaction. The 2-amino-6-mercapto-7-methylpurine product has an absorption peak at 360 nm, and coupled reactions catalyzed by Ppase and PNP are very rapid so the kinetics of DPPS, UPPS, and FPPS can be directly monitored at 360 nm. The total volume of each reaction was 200 μL, with a 100 μL reaction mixture being added to 100 μL of a protein mixture. Reactions were continuously monitored on a spectrophotometer at room temperature until there was no longer any significant increase in absorbance at 360 nm, indicating reaction completion. IPP, DMAPP, FPP, or *cis*-FPP substrate stock solutions (20 mM) were prepared in water. Basically, the same procedure was followed for inhibition assays except that prior to the addition of the reaction mixture to the protein mixture the protein was incubated with serial dilutions of the compound for 30 min at room temperature. Compound stock solutions in DMSO (10 mM) were used. All assays were performed at least three times on different days and with different inhibitor concentrations. For the active compounds in the single-point initial screen, dose−response curves were obtained and $IC_{50}$ values were calculated with GraphPad Prism software (version 7.04).

**MtDPPS Activity Assay, Inhibitor Screening, and $IC_{50}$ Determination.** The condensation of IPP and *cis*-FPP catalyzed by MtDPPS was monitored by using a continuous spectrophotometric assay for diphosphate release in 96-well plates with 200 μL reaction mixtures containing 400 μM MESG, 5 μM *cis*-FPP, 200 μM IPP, 25 mM Tris-HCl (pH 7.5), 0.01% Triton X-100, and 1 mM $MgCl_2$. Compounds from National Cancer Institute Diversity Set V were first screened at a single concentration, 50 μM. The $IC_{50}$ values for the most active compounds were then obtained using 15-point dose−response curves with data fitted to a rectangular hyperbolic dose−response function in OriginPro 8.5 (OriginLab, Northampton, MA).

**UPPS Assay.** The expression, purification, and storage of EcUPPS were as reported previously.[34] Assays were conducted at 25 °C in a reaction mixture of 50 μM IPP, 6 μM FPP, 63 nM EcUPPS, 0.3 unit of PNP, 0.6 unit of Ppase, and 0.1 mg/


https://dx.doi.org/10.1021/acsinfecdis.0c00472
ACS Infect. Dis. XXXX, XXX, XXX−XXX

mL MESG in activity buffer containing 100 mM HEPES (pH 7.5), 50 mM KCl, 0.5 mM $MgCl_2$, and 0.1% Triton X-100 (v/v). $IC_{50}$ values were determined using a four-parameter variable-slope function

$$Y = \text{bottom} + \frac{\text{top} - \text{bottom}}{1 + 10^{((\log IC_{50} - X) \times \text{Hillslope})}}$$

in the Prism program.

**FPPS Assay.** Expression, purification, and storage of HsFPPS were conducted as previously described.[39] Assays were performed at 25 °C using a mixture of 50 μM IPP and 50 μM GPP, 0.3 unit of PNP (Sigma-Aldrich, 10 units/mg), 0.6 unit of Ppase (Sigma-Aldrich, 500 units/mg), 0.1 mg/mL MESG, and 0.15 μM HsFPPS in a buffer containing 20 mM HEPES (pH 7.5), 150 mM NaCl, and 500 μM $MgCl_2$. $IC_{50}$ values were determined using a four-parameter variable-slope function

$$Y = \text{bottom} + \frac{\text{top} - \text{bottom}}{1 + 10^{((\log IC_{50} - X) \times \text{Hillslope})}}$$

in the Prism program.

***B. subtilis* Growth Inhibition Assay.** An overnight starter culture (in LB both) of *B. subtilis* was diluted 1000-fold (in fresh LB media) and grown to an $OD_{600}$ of ∼0.3 (approximately 3.5 h at 37 °C). This log-phase culture was then diluted 500-fold into fresh LB broth to generate the working solution. This working solution (180 μL) was then transferred into every well in a flat-bottom 96-well plate except for the first column. Inhibitors were added at specific starting concentrations (100 μM−1 mM) with a total volume of 360 μL (diluted with working solution) into the first column. The inhibitors were then sequentially diluted 2-fold across 12 wells. Plates were incubated at 37 °C and shaken at 200 rpm for 12 h. The $OD_{600}$ values were then measured to determine $IC_{50}$ values using GraphPad Prism software (version 7.04). Experiments were carried out in duplicate or triplicate. $IC_{50}$ values were determined using a four-parameter variable-slope function

$$Y = \text{bottom} + \frac{\text{top} - \text{bottom}}{1 + 10^{((\log IC_{50} - X) \times \text{Hillslope})}}$$

in the Prism program.

***B. subtilis* Cell Growth Inhibition Rescue Assays.** An overnight starter culture (in LB both) of *B. subtilis* was diluted 1000-fold (in fresh LB media) and grown to an $OD_{600}$ value of ∼0.3 (approximately 3.5 h at 37 °C). The working solution was prepared by 500-fold dilution of this log-phase culture into fresh LB broth. Then, 50 μM solutions of UP, MK-4, or both were prepared using the 500-fold diluted working solution; 200 μL of working solution was then transferred into every well in a flat-bottom 96-well plate, except for the first column. Inhibitors were added at specific starting concentrations (100 μM−1 mM) with a total volume of 300 μL (diluted with working solution) into the first column. The inhibitors were then sequentially diluted 3-fold across 12 wells. Plates were incubated at 37 °C with shaking at 200 rpm for 12 h. The $OD_{600}$ values were then measured to determine bacterial growth inhibition rescue effects, basically as described above for *B. subtilis* alone.

***S. aureus* Growth Inhibition Assay.** An overnight starter culture of *S. aureus* was diluted 1000-fold (in fresh Tryptic soy media or LB broth) and grown to an $OD_{600}$ value of ∼0.3 (approximately 3.5 h at 37 °C). This log-phase culture was diluted 500-fold into fresh tryptic soy broth or LB broth to generate the working solution. This working solution (180 or 30 μL) was then transferred into every well in a flat-bottom 96-well plate or a flat-bottom 384-well plate, except for the first column. Inhibitors were added at specific starting concentrations (100 μM−1 mM or 0.04−83 μg/mL) with a total volume of 360 or 60 μL (diluted with working solution) to the first column. The inhibitors were then sequentially diluted 2-fold across 12 wells. Plates were incubated at 37 °C, with shaking at 200 rpm for ∼12−24 h. The $OD_{600}$ values were then measured to determine the bacterial growth inhibition.

***B. anthracis* Sterne Growth Inhibition Assay.** An overnight starter culture of *B. anthracis* Sterne was diluted 1000-fold (in fresh Mueller-Hinton Broth 2 media) and grown to an $OD_{600}$ value of ∼0.3 (approximately 3.5 h at 37 °C). This log-phase culture was diluted 500-fold into fresh MHB broth to generate the working solution. This working solution (180 μL) was then transferred into every well in a flat-bottom 96-well plate, except for the first column. Inhibitors were added at specific starting concentrations (100 μM−1 mM) with a total volume of 360 μL (diluted with working solution) into the first column. The inhibitors were then sequentially diluted 2-fold across 12 wells. Plates were incubated at 37 °C with shaking at 200 rpm for 12 h. The $OD_{600}$ value was then measured to determine bacterial growth inhibition.

***M. smegmatis* growth inhibition assay.** *M. smegmatis* (grown for 36−48 h) was diluted 1000-fold in fresh Middlebrook 7H9 (plus 10% ADC supplement, Sigma: M0553-1VL; 0.5% glycerol; 0.05% Tween 80) media to generate a working solution. This working solution (180 μL) was then transferred into every well in a flat-bottomed 96-well plate except for the second column and peripheral wells. Inhibitors were added at specific starting concentrations (100 μM−1 mM) with a total volume of 300 μL (diluted with working solution) to the second column. The inhibitors were then sequentially diluted 3-fold across 10 wells; 200 μL of water was added to each peripheral well to prevent water evaporation from the plate. Plates were incubated at 37 °C, with shaking at 200 rpm for 48 h. The $OD_{600}$ values were then measured to determine bacterial growth inhibition, as described above.

**Determination of the Minimum Inhibitory Concentrations (MICs) against *C. difficile*.** MICs of the tested compounds were determined against *C. difficile* as described previously.[40−43] Briefly, *C. difficile* strains were grown anaerobically on brain−heart infusion-supplemented agar plates (brain−heart infusion medium, BD, supplemented with yeast extract, L-cysteine, vitamin K1, and hemin) at 37 °C for 48 h. Then, a bacterial solution equivalent to a 0.5 McFarland standard was prepared and diluted in brain−heart infusion-supplemented broth to achieve a bacterial concentration of ∼$5 \times 10^5$ CFU/mL, and cells were then seeded into 96-well well plates. Inhibitors were added and serially diluted along the plates. Plates were then incubated anaerobically at 37 °C for 48 h. MIC values reported are the minimum concentrations of the inhibitor that completely inhibited cell growth as measured from serial 2-fold dilutions and are the averages of at least two experiments.

***E. coli* Growth-Inhibition Assay.** An overnight starter culture of *E. coli* (K12) was diluted 1000-fold and grown to an $OD_{600}$ value of ∼0.3. These log-phase cultures were then diluted 500-fold into fresh LB broth to generate a working


https://dx.doi.org/10.1021/acsinfecdis.0c00472
ACS Infect. Dis. XXXX, XXX, XXX−XXX

solution. Working solution (200 μL) was transferred into each well of a 96-well culture plate. Inhibitors were then addedat 1 mM and sequentially diluted 3-fold to 46 nM, keeping the volume and culture broth composition constant. Plates were incubated for 12 h at 37 °C with shaking at 200 rpm. The $OD_{600}$ value was then measured to determine bacterial growth inhibition.

**Other Gram-Negative Bacterial Cell Growth Inhibition Assays.** As with the *E. coli* inhibition assays, overnight cultures (in cation-adjusted Mueller-Hinton broth, CAMHB) of *A. baumannii*, *K. pneumoniae*, and *P. aeruginosa* were diluted 1000-fold (in fresh CAMHB) to create a working solution. Working solutions were then transferred into flat-bottomed 96-well plates and inhibitors were added at 1 mM and sequentially diluted 3-fold to 46 nM. Plates were incubated at 37 °C with shaking at 200 rpm overnight. $OD_{600}$ values were then measured to determine bacterial growth inhibition.

**FDA-Approved Antibiotics Synergy Screening.** FDA-approved antibiotics (174) from the FDA compound library (Selleck Chemicals, Houston, TX) were used for a synergy screening. An overnight culture of *S. aureus* Newman was diluted to $5 \times 10^5$ CFU/mL to prepare the working solution of bacteria in LB broth with $^1/_2$ MIC of redoxal (**10**). Working solution (30 μL) was added to each well of a sterile 384-well plate, and compounds from the library were serial 2-fold diluted to generate various concentrations. Four wells with **10** but without antibiotics were used as controls. The wells with no **10** or antibiotics were used as positive controls, and the wells with LB broth only were set as negative controls. Then, the plate was incubated at 37 °C at 220 rpm, and the $OD_{600}$ of each well was determined after 24 h using a microplate reader. The fold decrease was MIC = MIC(antibiotic only)/MIC(antibiotic + $^1/_2$ MIC **10**).

**Resistance Development Assays.** The assay for resistance development was determined as previously reported.[44] In brief, the method for MIC determination against *S. aureus* Newman was repeated daily for 14 passages (i.e., over a 2 week period). The initial working solution contained $5 \times 10^5$ CFU/mL bacteria in LB broth. For each subsequent passage, the inoculum for MIC determination was adjusted to a final density of approximately $5 \times 10^5$ CFU/mL using the contents of a well containing **10** or kanamycin at a subinhibitory concentration. To measure the MIC of each passage, bacteria were transferred to a new 96-well microtiter plate, and then compounds were added.

**Sensitization Assay with Pentamidine.** Pentamidine has been reported as a sensitizer to potentiate some antibiotics for inhibiting *E. coli* or *A. baumannii*, so we combined **10** or **17** with $^1/_2$ MIC or $^1/_4$ MIC pentamidine against *A. baumannii*. An overnight culture of *A. baumannii* was diluted in fresh CAMHB broth to generate a solution containing $5 \times 10^5$ CFU/mL bacteria, and then 256 μg/mL ($^1/_2$ MIC) or 128 μg/mL (1/4 MIC) pentamidine was added to generate a working solution. Working solution (100 μL) was transferred into each well of a 96-well culture plate. **10** or **17** was then added at 32 or 16 μg/mL and sequentially diluted 2-fold, keeping the volume and culture broth composition constant. Plates were incubated for 24 h at 37 °C with shaking at 220 rpm. The $OD_{600}$ value was then measured to determine the bacterial growth inhibition.

**Inverted Membrane Vesicles (IMVs).** The preparation of IMVs was the same as reported previously.[45] In brief, *E. coli* IMVs were prepared by three passages through a precooled French pressure cell at 20 000 psi. The lysate was centrifuged at 14 000*g* at 4 °C for 20 min to remove unbroken cells. The supernatant was centrifuged at 370 000*g* at 4 °C for 1 h, and the pellet, consisting of the IMVs, was washed with 50 mM MOPS−KOH (pH 7.5) and 2 mM $MgCl_2$. After the second centrifugation step, membranes were resuspended in a solution of 50 mM MOPS−KOH (pH 7.5), 2 mM $MgCl_2$, and 10% glycerol and stored at −80 °C.

**Assay for ATP or Succinate-Driven Proton Translocation.** Proton translocation into IMVs was measured by the decrease in ACMA fluorescence as previously reported.[45] The excitation and emission wavelengths were 410 and 480 nm, respectively. IMVs (0.1 mg/mL membrane protein) were preincubated at 37 °C in a solution of 10 mM HEPES−KOH (pH 7.5), 100 mM KCl, and 5 mM $MgCl_2$ containing 2 μM ACMA, and the baseline was monitored for 5 min. The reaction was then initiated by adding 1 mM ATP or 5 mM succinate. When the signal had stabilized, **10** was added and proton translocation was measured fluorometrically. $IC_{50}$ values were determined using a four-parameter variable-slope function:

$$Y = \text{bottom} + \frac{\text{top} - \text{bottom}}{1 + 10^{((\log IC_{50} - X) \times \text{Hillslope})}}$$

in the Prism program.

**Cell Growth Inhibition Assay.** The cytotoxicity of the **10** was evaluated with human embryonic kidney 293 cells (HEK293T) and mouse embryonic fibroblast cells (NIH/3T3) by using the MTT cell viability assay. In brief, HEK293T or NIH/3T3 cells were suspended in medium containing Dulbecco's modified Eagle's medium (DMEM), 10% fetal bovine serum (FBS), 4.5 g/L D-glucose, 1% L-glutamine, and 110 mg/L sodium pyruvate. HEK293T or NIH/3T3 (100 μL, $1.0 \times 10^5$ cells/mL) was seeded in a 96-well microtiter plate and incubated for 12 h at 37 °C in 5% $CO_2$. **10** was gradient diluted in advance in PBS (1×), and at the end of the preincubation, **10** was added to the original medium ranging from 0.5 to 64 or 3−344 μM for 24 h. After incubation, the medium was removed and each well was washed twice with PBS (1×). Then, 120 μL of 0.5 mg/mL MTT in DMEM without FBS was added to each well and incubated for 1.5 h. Next, the DMEM with MTT was discarded and 100 μL of dimethyl sulfoxide (DMSO) per well was added to the 96-well plate to dissolve formazan crystals. The absorbance of the color was measured at 600 nm. A negative control of untreated cells was also analyzed in each experiment, and the experiment was repeated three times. $IC_{50}$ values were determined by using a two-parameter fit in the Prism program

$$Y = \frac{100}{1 + 10^{((\log IC_{50} - X) \times \text{Hillslope})}}$$

**Hemolysis Assay.** Fresh sheep red blood cells (RBCs) were diluted with 1× PBS to achieve a final concentration of 4%. Then, 150 μL of sample containing various concentrations of **10** was incubated in a 96-well plate at 37 °C and 220 rpm for 1 h. After incubation, the mixtures were centrifuged at 1000 rpm for 10 min, and aliquots (100 μL) of supernatant were transferred to a 96-well plate. Hemoglobin release was determined by measuring the absorbance at 576 nm. Triton X-100 (0.2%) was used as the positive control; 4% RBCs in 1× PBS alone were used as the negative control. The percent of hemolysis was calculated as follows:


https://dx.doi.org/10.1021/acsinfecdis.0c00472
ACS Infect. Dis. XXXX, XXX, XXX−XXX

$$\%\,\text{hemolysis} = \frac{\text{Abs}_{\text{sample}} - \text{Abs}_{\text{negative control}}}{\text{Abs}_{\text{positive control}} - \text{Abs}_{\text{negative control}}} \times 100\%$$

***In Vivo* Toxicity Test with *C. elegans*.** This animal study was performed in accordance with national regulations on animal studies. To assess the *in vivo* toxicity of redoxal, the *C. elegans* (N2) whole animal model was used. Briefly, hatched larvae were transferred onto an NGM plate seeded with *E. coli* OP50 and incubated at 25 °C for 2 to 3 days until *C. elegans* reached L4. Next, worms were collected and washed with PBS (1×) three times to remove OP50. Redoxal solutions with different concentrations (128, 64, 32, and 16 μg/mL) were added to the centrifuge tubes, and the worms were incubated for 24 h at 20 °C. Worm survival was observed with a microscope. Each concentration group included three independent replicates.

***In Vivo* Antimicrobial Evaluation with *C. elegans*.** This animal study was performed in accordance with national regulations on animal studies. To assess the antimicrobial efficacy of redoxal against *S. aureus* infection *in vivo*, L4 *C. elegans* worms were collected and washed with PBS (1×) three times to remove OP50. To establish the infected animal model, adult-stage worms (L4) were transferred onto TSA agar plates and seeded with a lawn of *S. aureus* (Newman strain) for infection. After 6 h, worms were collected and washed with PBS three times, and then 10 worms per well were transferred into 96-well microtiter plates. Worms were incubated with 16 μM ofredoxal, 54 μM ampicillin (positive control), or PBS (negative control) in triplicate. After treatment with test agents for 8 h, worms were washed three times with PBS and then examined for morphological changes and viability using a light microscope. Next, worms were ground with a glass rod in microcentrifuge tubes containing 200 mg of 1.0 mm silicon carbide particles (Biospec Products, Bartlesville, OK). After vortex mixing for 1 min, the samples were gradient-diluted and then plated onto TSA agar plates (90 mm) containing 5 μg/mL nalidixic acid to select for *S. aureus* growth. Plates were incubated at 37 °C for 12 h to determine the CFU/mL. The experiment was repeated three times. Data were analyzed using GraphPad Prism software (version 7.04) using a two-parameter fit.

**Molecular Docking.** We docked the best MtDPPS inhibitor (**10**) to MtDPPS, SaUPPS, EcUPPS, and HsFPPS using the X-ray crystallographic structures indicated in the text. For each structure, the receptors were protonated using the Protonate3D module[46] of the MOE.[47] In brief, we used the generalized Born/volume integral (GB/VI) model of hydration[48] with electrostatic interactions treated with Coulomb's law and a cutoff of 15 Å and a dielectric of 2 inside of protein. van der Waals interactions were treated with the 800R3 potential and a cutoff of 10 Å. Implicit solvent was used with a dielectric of 80. The temperature set to 300 K at pH 7.0 and a salt concentration of 0.1 mM. Partial charges were assigned using the Amber 10 force field. For the ligand, the initial coordinates and structure of **10** were predicted from the chemical structure (CML file) using Avogadro v. 1.2.0.[49] The structure was protonated with the Protonate3D program and solvated in a sphere of explicit all-atom water molecules, and its energy was minimized in MOE, again using the Amber 10 force field. The resulting structure was extracted and used for docking. Docking was carried out using the MOE docking function.

**Statistical Analysis.** The $Z'$ factor was calculated using the following equation, where the term $|\mu_{c+} - \mu_{c-}|$ represents the difference between the mean of the positive and negative controls and $\sigma_{c+}$ and $\sigma_{c-}$ indicate the standard deviations for the positive and negative controls, respectively.

$$Z'\text{ factor} = 1 - \frac{(3\sigma_{c+} + 3\sigma_{c-})}{|\mu_{c+} - \mu_{c-}|}$$

The coefficient of variation (CV) was calculated using the equation CV = $\sigma/\mu$, where $\sigma$ represents the standard deviation and $\mu$ represents the mean.

## ■ ASSOCIATED CONTENT

### Supporting Information

The Supporting Information is available free of charge at https://pubs.acs.org/doi/10.1021/acsinfecdis.0c00472.

SDS-PAGE gel showing purity, MESG activity assay, and enzyme activity of MtDPPS; chemical structures of the MtDPPS inhibitors with $IC_{50}$ values; molecular electrostatic potential surface of FPP and MtDPPS inhibitors possessing charge-hydrophobic scaffolds; dose-response curves for *E. coli* UPPS and human FPPS inhibition by redoxal; docking results for redoxal/EcUPPS; MtDPPS, SaUPPS, EcUPPS, and HsFPPS protein-10 interactions; correlations between DPPS inhibition and two descriptors; FDA-approved antibiotics synergy screening with $^1/_2$ MIC **10**; pentamidine sensitization results; $IC_{50}$ fitting curves for HEK293T cell and NIH/3T3 cell growth inhibition of 10; $LD_{50}$ of **10** for *C. elegans*; qNMR results for **10**; qNMR results for **17**; activity of 10 against S. aureus clinical strains; and FDA approved antibiotics synergy screening results with $^1/_2$ MIC **10** (PDF)

## ■ AUTHOR INFORMATION


### Corresponding Authors

**Eric Oldfield** − *Department of Chemistry, University of Illinois at Urbana—Champaign, Urbana, Illinois 61801, United States;* orcid.org/0000-0002-0996-7352; Phone: (217) 333-3374; Email: eoldfiel@illinois.edu

**Xinxin Feng** − *Institute of Chemical Biology and Nanomedicine, State Key Laboratory of Chemo/Biosensing and Chemometrics, Hunan Provincial Key Laboratory of Biomacromolecular Chemical Biology, and Department of Chemistry, Hunan University, Changsha 410082, China;* orcid.org/0000-0003-3142-5629; Phone: 86-13272001426; Email: xinxin_feng@hnu.edu.cn

### Authors

**Junfeng Song** − *Institute of Chemical Biology and Nanomedicine, State Key Laboratory of Chemo/Biosensing and Chemometrics, Hunan Provincial Key Laboratory of Biomacromolecular Chemical Biology, and Department of Chemistry, Hunan University, Changsha 410082, China*

**Satish R. Malwal** − *Department of Chemistry, University of Illinois at Urbana—Champaign, Urbana, Illinois 61801, United States;* orcid.org/0000-0001-7606-1932

**Noman Baig** − *Department of Chemistry, University of Illinois at Urbana—Champaign, Urbana, Illinois 61801, United States*

**Lici A. Schurig-Briccio** − *Department of Biochemistry, University of Illinois at Urbana—Champaign, Urbana, Illinois 61801, United States*




https://dx.doi.org/10.1021/acsinfecdis.0c00472
ACS Infect. Dis. XXXX, XXX, XXX−XXX

**Zijun Gao** − *Department of Chemistry, University of Illinois at Urbana—Champaign, Urbana, Illinois 61801, United States*
**Girija S. Vaidya** − *Department of Chemistry, University of Illinois at Urbana—Champaign, Urbana, Illinois 61801, United States*
**Kailing Yang** − *Institute of Chemical Biology and Nanomedicine, State Key Laboratory of Chemo/Biosensing and Chemometrics, Hunan Provincial Key Laboratory of Biomacromolecular Chemical Biology, and Department of Chemistry, Hunan University, Changsha 410082, China*
**Nader S. Abutaleb** − *Department of Comparative Pathobiology, College of Veterinary Medicine, Purdue University, West Lafayette, Indiana 47907, United States;* orcid.org/0000-0003-1730-4150
**Mohamed N. Seleem** − *Department of Comparative Pathobiology, College of Veterinary Medicine, Purdue University, West Lafayette, Indiana 47907, United States; Department of Biomedical Sciences and Pathobiology, Virginia-Maryland College of Veterinary Medicine, Virginia Polytechnic Institute and State University, Blacksburg, Virginia 24061, United States;* orcid.org/0000-0003-0939-0458
**Robert B. Gennis** − *Department of Chemistry and Department of Biochemistry, University of Illinois at Urbana—Champaign, Urbana, Illinois 61801, United States;* orcid.org/0000-0002-3805-6945
**Taras V. Pogorelov** − *Department of Chemistry, Center for Biophysics and Quantitative Biology, National Center for Supercomputing Applications, Beckman Institute for Advanced Science and Technology, and School of Chemical Sciences, University of Illinois at Urbana—Champaign, Urbana, Illinois 61801, United States;* orcid.org/0000-0001-5851-7721

Complete contact information is available at: https://pubs.acs.org/10.1021/acsinfecdis.0c00472

### Author Contributions

J.S., N.S.A., and M.N.S. performed bacterial growth inhibition and cell toxicity assays. S.R.M., N.B., Z.G., and G.S.V. synthesized enzyme substrates, purified redoxal, and performed enzyme inhibition assays and additional cell growth inhibition assays. T.V.P. performed the docking studies. L.A.S.-B., and R.B.G. investigated the uncoupling activity. K.Y. performed the *C. elegans* infection assay. E.O. and X.F. wrote the article.

### Notes

The authors declare no competing financial interest.

## ■ ACKNOWLEDGMENTS

This work was supported in part by the National Natural Science Foundation of China (grant 21807031), the Open Funding Project of the State Key Laboratory of Biocatalysis and Enzyme Engineering (SKLBEE2019003), the Fundamental Research Funds for the Central Universities from Hunan University (China) to X.F., and the United States Public Health Service (National Institutes of Health grants GM065307 and CA158191) to E.O. We thank Professor Douglas A. Mitchell and Professor Zhi Su for providing bacteria.

## ■ ABBREVIATIONS

DPPS, decaprenyl diphosphate synthase; FPPS, farnesyl diphosphate synthase; UPPS, undecaprenyl diphosphate synthase; *cis*-PT, *cis*-prenyltransferase; IPP, isopentenyl diphosphate; DMAPP, dimethylallyl diphosphate; FPP, farnesyl diphosphate; UPP, undecaprenyl diphosphate; MK, menaquinone; DP, decaprenyl phosphate; UP, undecaprenyl phosphate; $IC_{50}$, half-maximal inhibitory concentration; MIC, minimum inhibitory concentration; Bs, *B. subtilis*; Ba, *B. anthracis* Sterne; Sa, *S. aureus*; Ms, *M. smegmatis*; HEK293T, human embryonic kidney cell line no. 293T; NIH/3T3, mouse embryonic fibroblast cell line; MESG, 2-amino-6-mercapto-7-methylpurine; MTT, 3-(4,5-dimethyl-2-thiazolyl)-2,5-diphenyl-2*H*-tetrazolium bromide; ACMA, 9-amino-6-chloro-9-amino-6-chloro-2-methoxyacridine; CCCP, *m*-chlorophenylcarbonyl cyanide phenylhydrazone

## ■ REFERENCES

(1) World Health Organization. Global Tuberculosis Report 2017.
(2) Kohanski, M. A., Dwyer, D. J., and Collins, J. J. (2010) How antibiotics kill bacteria: from targets to networks. *Nat. Rev. Microbiol. 8* (6), 423−435.
(3) Zhu, W., Zhang, Y., Sinko, W., Hensler, M. E., Olson, J., Molohon, K. J., Lindert, S., Cao, R., Li, K., Wang, K., Wang, Y., Liu, Y.-L., Sankovsky, A., de Oliveira, C. A. F., Mitchell, D. A., Nizet, V., McCammon, J. A., and Oldfield, E. (2013) Antibacterial drug leads targeting isoprenoid biosynthesis. *Proc. Natl. Acad. Sci. U. S. A. 110* (1), 123−128.
(4) Sinko, W., Wang, Y., Zhu, W., Zhang, Y., Feixas, F., Cox, C. L., Mitchell, D. A., Oldfield, E., and McCammon, J. A. (2014) Undecaprenyl diphosphate synthase inhibitors: antibacterial drug leads. *J. Med. Chem. 57* (13), 5693−5701.
(5) Wang, Y., Desai, J., Zhang, Y., Malwal, S. R., Shin, C. J., Feng, X., Sun, H., Liu, G., Guo, R.-T., and Oldfield, E. (2016) Bacterial cell gowth inhibitors targeting undecaprenyl diphosphate synthase and undecaprenyl diphosphate phosphatase. *ChemMedChem 11* (20), 2311−2319.
(6) Concha, N., Huang, J., Bai, X., Benowitz, A., Brady, P., Grady, L. C., Kryn, L. H., Holmes, D., Ingraham, K., Jin, Q., Pothier Kaushansky, L., McCloskey, L., Messer, J. A., O'Keefe, H., Patel, A., Satz, A. L., Sinnamon, R. H., Schneck, J., Skinner, S. R., Summerfield, J., Taylor, A., Taylor, J. D., Evindar, G., and Stavenger, R. A. (2016) Discovery and characterization of a class of pyrazole inhibitors of bacterial undecaprenyl pyrophosphate synthase. *J. Med. Chem. 59* (15), 7299−304.
(7) Guo, R.-T., Cao, R., Liang, P.-H., Ko, T.-P., Chang, T.-H., Hudock, M. P., Jeng, W.-Y., Chen, C. K. M., Zhang, Y., Song, Y., Kuo, C.-J., Yin, F., Oldfield, E., and Wang, A. H. J. (2007) Bisphosphonates target multiple sites in both *cis*- and *trans*-prenyltransferases. *Proc. Natl. Acad. Sci. U. S. A. 104* (24), 10022−10027.
(8) Chan, H. C., Feng, X., Ko, T. P., Huang, C. H., Hu, Y., Zheng, Y., Bogue, S., Nakano, C., Hoshino, T., Zhang, L., Lv, P., Liu, W., Crick, D. C., Liang, P. H., Wang, A. H., Oldfield, E., and Guo, R. T. (2014) Structure and inhibition of tuberculosinol synthase and decaprenyl diphosphate synthase from *Mycobacterium tuberculosis*. *J. Am. Chem. Soc. 136* (7), 2892−2896.
(9) Zhang, J.-H., Chung, T. D., and Oldenburg, K. R. (1999) A simple statistical parameter for use in evaluation and validation of high throughput screening assays. *J. Biomol. Screening 4* (2), 67−73.
(10) Jahnke, W., Rondeau, J.-M., Cotesta, S., Marzinzik, A., Pelle, X., Geiser, M., Strauss, A., Goette, M., Bitsch, F., Hemmig, R., Henry, C., Lehmann, S., Glickman, J. F., Roddy, T. P., Stout, S. J., and Green, J. R. (2010) Allosteric non-bisphosphonate FPPS inhibitors identified by fragment-based discovery. *Nat. Chem. Biol. 6* (9), 660−666.
(11) Baell, J. B., and Holloway, G. A. (2010) New substructure filters for removal of Pan Assay Interference Compounds (PAINS) from screening libraries and for their exclusion in bioassays. *J. Med. Chem. 53* (7), 2719−2740.
(12) Bonnett, S. A., Ollinger, J., Chandrasekera, S., Florio, S., O'Malley, T., Files, M., Jee, J.-A., Ahn, J., Casey, A., Ovechkina, Y., Roberts, D., Korkegian, A., and Parish, T. (2016) A target-based whole cell screen approach to identify potential inhibitors of

*Mycobacterium tuberculosis* signal peptidase. *ACS Infect. Dis. 2* (12), 893−902.
(13) Park, J., Zielinski, M., Magder, A., Tsantrizos, Y. S., and Berghuis, A. M. (2017) Human farnesyl pyrophosphate synthase is allosterically inhibited by its own product. *Nat. Commun. 8* (1), 14132.
(14) Liu, Y.-L., Cao, R., Wang, Y., and Oldfield, E. (2015) Farnesyl diphosphate synthase inhibitors with unique ligand-binding geometries. *ACS Med. Chem. Lett. 6* (3), 349−354.
(15) Han, S., Li, X., Xia, Y., Yu, Z., Cai, N., Malwal, S. R., Han, X., Oldfield, E., and Zhang, Y. (2019) Farnesyl pyrophosphate synthase as a target for drug development: discovery of natural-product-derived inhibitors and their activity in pancreatic cancer cells. *J. Med. Chem. 62* (23), 10867−10896.
(16) Mukkamala, D., No, J. H., Cass, L. A., Chang, T.-K., and Oldfield, E. (2008) Bisphosphonate inhibition of a plasmodium farnesyl diphosphate synthase and a general method for predicting cell-based activity from enzyme data. *J. Med. Chem. 51* (24), 7827−7833.
(17) Richter, M. F., Drown, B. S., Riley, A. P., Garcia, A., Shirai, T., Svec, R. L., and Hergenrother, P. J. (2017) Predictive compound accumulation rules yield a broad - spectrum antibiotic. *Nature 545* (7654), 299−304.
(18) Tsai, F. T. F., Singh, O. M. P., Skarzynski, T., Wonacott, A. J., Weston, S., Tucker, A., Pauptit, R. A., Breeze, A. L., Poyser, J. P., O'Brien, R., Ladbury, J. E., and Wigley, D. B. (1997) The high-resolution crystal structure of a 24-kDa gyrase B fragment from *E. coli* complexed with one of the most potent coumarin inhibitors, clorobiocin. *Proteins: Struct., Funct., Genet. 28* (1), 41−52.
(19) Liu, J., Lee, J., Hernandez, M. A. S., Mazitschek, R., and Ozcan, U. (2015) Treatment of obesity with celastrol. *Cell 161* (5), 999−1011.
(20) Yang, C., Swallows, C. L., Zhang, C., Lu, J., Xiao, H., Brady, R. O., and Zhuang, Z. (2014) Celastrol increases glucocerebrosidase activity in Gaucher disease by modulating molecular chaperones. *Proc. Natl. Acad. Sci. U. S. A. 111* (1), 249−254.
(21) Song, J., Shang, N., Baig, N., Yao, J., Shin, C., Kim, B. K., Li, Q., Malwal, S. R., Oldfield, E., Feng, X., and Guo, R.-T. (2019) *Aspergillus flavus* squalene synthase as an antifungal target: Expression, activity, and inhibition. *Biochem. Biophys. Res. Commun. 512* (3), 517−523.
(22) Klaic, L., Trippier, P. C., Mishra, R. K., Morimoto, R. I., and Silverman, R. B. (2011) Remarkable stereospecific conjugate additions to the Hsp90 inhibitor celastrol. *J. Am. Chem. Soc. 133* (49), 19634−19637.
(23) Lu, S., Tian, J., Sun, W., Meng, J., Wang, X., Fu, X., Wang, A., Lai, D., Liu, Y., and Zhou, L. (2014) Bis-naphtho-γ-pyrones from Fungi and Their Bioactivities. *Molecules 19* (6), 7169−7188.
(24) Qiang, G., Xue, S., Yang, J. J., Du, G., Pang, X., Li, X., Goswami, D., Griffin, P. R., Ortlund, E. A., Chan, C. B., and Ye, K. (2014) Identification of a small molecular insulin receptor agonist with potent antidiabetes activity. *Diabetes 63* (4), 1394−1409.
(25) Mori, S., Kawai, K., Nozawa, Y., Koyama, K., and Natori, S. (1993) The impairing effects of chaetochromin D on mitochondrial respiration and structure. *Mycotoxin Res. 9* (2), 85−93.
(26) Knecht, W., and Loffler, M. (2000) Redoxal as a new lead structure for dihydroorotate dehydrogenase inhibitors: a kinetic study of the inhibition mechanism. *FEBS Lett. 467* (1), 27−30.
(27) Crona, M., Codo, P., Jonna, V. R., Hofer, A., Fernandes, A. P., and Tholander, F. (2016) A ribonucleotide reductase inhibitor with deoxyribonucleoside-reversible cytotoxicity. *Mol. Oncol. 10* (9), 1375−1386.
(28) Lee, M.-H. H., Graham, G. G., Williams, K. M., and Day, R. O. (2008) A benefit-risk assessment of benzbromarone in the treatment of gout. *Drug Saf. 31* (8), 643−665.
(29) Younis, W., AbdelKhalek, A., Mayhoub, A. S., and Seleem, M. N. (2017) *In vitro* screening of an FDA-approved library against ESKAPE pathogens. *Curr. Pharm. Des. 23* (14), 2147−2157.
(30) Ejim, L., Farha, M. A., Falconer, S. B., Wildenhain, J., Coombes, B. K., Tyers, M., Brown, E. D., and Wright, G. D. (2011) Combinations of antibiotics and nonantibiotic drugs enhance antimicrobial efficacy. *Nat. Chem. Biol. 7* (6), 348−350.
(31) Murray, E. J., Crowley, R. C., Truman, A., Clarke, S. R., Cottam, J. A., Jadhav, G. P., Steele, V. R., O'Shea, P., Lindholm, C., Cockayne, A., Chhabra, S. R., Chan, W. C., and Williams, P. (2014) Targeting *staphylococcus aureus* quorum sensing with nonpeptidic small molecule inhibitors. *J. Med. Chem. 57* (6), 2813−2819.
(32) Stokes, J. M., MacNair, C. R., Ilyas, B., French, S., Cote, J.-P., Bouwman, C., Farha, M. A., Sieron, A. O., Whitfield, C., Coombes, B. K., and Brown, E. D. (2017) Pentamidine sensitizes gram-negative pathogens to antibiotics and overcomes acquired colistin resistance. *Nat. Microbiol. 2* (5), 17028.
(33) Malwal, S. R., Chen, L., Hicks, H., Qu, F., Liu, W., Shillo, A., Law, W. X., Zhang, J., Chandnani, N., Han, X., Zheng, Y., Chen, C. C., Guo, R. T., AbdelKhalek, A., Seleem, M. N., and Oldfield, E. (2019) Discovery of lipophilic bisphosphonates that target bacterial cell wall and quinone biosynthesis. *J. Med. Chem. 62* (5), 2564−2581.
(34) Feng, X., Zhu, W., Schurig-Briccio, L. A., Lindert, S., Shoen, C., Hitchings, R., Li, J., Wang, Y., Baig, N., Zhou, T., Kim, B. K., Crick, D. C., Cynamon, M., McCammon, J. A., Gennis, R. B., and Oldfield, E. (2015) Antiinfectives targeting enzymes and the proton motive force. *Proc. Natl. Acad. Sci. U. S. A. 112* (51), E7073−E7082.
(35) Felser, A., Lindinger, P. W., Schnell, D., Kratschmar, D. V., Odermatt, A., Mies, S., Jenoe, P., and Kraehenbuehl, S. (2014) Hepatocellular toxicity of benzbromarone: Effects on mitochondrial function and structure. *Toxicology 324*, 136−146.
(36) Zhang, B., Li, J., Yang, X., Wu, L., Zhang, J., Yang, Y., Zhao, Y., Zhang, L., Yang, X., Yang, X., Cheng, X., Liu, Z., Jiang, B., Jiang, H., Guddat, L. W., Yang, H., and Rao, Z. (2019) Crystal structures of membrane transporter MmpL3, an anti-TB drug target. *Cell 176* (3), 636−648.
(37) Gange, D. M. D. S., Lopata, R. J., and Henegar, K. (1995) The QSAR of insecticidal uncouplers. *Classical and Three-Dimensional QSAR in Agrochemistry*; ACS Symposium Series; Hansch, C., and Fujita, T., Eds.; Vol. *606*, pp 199−212.
(38) Webb, M. R. (1992) A continuous spectrophotometric assay for inorganic phosphate and for measuring phosphate release kinetics in biological systems. *Proc. Natl. Acad. Sci. U. S. A. 89* (11), 4884−4887.
(39) Kavanagh, K. L., Guo, K., Dunford, J. E., Wu, X., Knapp, S., Ebetino, F. H., Rogers, M. J., Russell, R. G. G., and Oppermann, U. (2006) The molecular mechanism of nitrogen-containing bisphosphonates as anti osteoporosis drugs. *Proc. Natl. Acad. Sci. U. S. A. 103* (20), 7829−7834.
(40) Abutaleb, N. S., and Seleem, M. N. (2020) Repurposing the antiamoebic drug diiodohydroxyquinoline for treatment of *Clostridioides difficile* Infections. *Antimicrob. Agents Chemother. 64* (6), e02115-19.
(41) Mody, D., Athamneh, A. I. M., and Seleem, M. N. (2020) Curcumin: A natural derivative with antibacterial activity against *Clostridium difficile*. *J. Glob. Antimicrob. Resist. 21*, 154−161.
(42) Pal, R., and Seleem, M. N. (2020) Screening of natural products and approved oncology drug libraries for activity against *Clostridioides difficile*. *Sci. Rep. 10* (1), 5966.
(43) AbdelKhalek, A., Abutaleb, N. S., Mohammad, H., and Seleem, M. N. (2019) Antibacterial and antivirulence activities of auranofin against *Clostridium difficile*. *Int. J. Antimicrob. Agents 53* (1), 54−62.
(44) Mwangi, J., Yin, Y., Wang, G., Yang, M., Li, Y., Zhang, Z., and Lai, R. (2019) The antimicrobial peptide ZY4 combats multidrug-resistant Pseudomonas aeruginosa and Acinetobacter baumannii infection. *Proc. Natl. Acad. Sci. U. S. A. 116* (52), 26516−26522.
(45) Li, K., Schurig-Briccio, L. A., Feng, X., Upadhyay, A., Pujari, V., Lechartier, B., Fontes, F. L., Yang, H., Rao, G., Zhu, W., Gulati, A., No, J. H., Cintra, G., Bogue, S., Liu, Y.-L., Molohon, K., Orlean, P., Mitchell, D. A., Freitas-Junior, L., Ren, F., Sun, H., Jiang, T., Li, Y., Guo, R.-T., Cole, S. T., Gennis, R. B., Crick, D. C., and Oldfield, E. (2014) Multitarget Drug Discovery for Tuberculosis and Other Infectious Diseases. *J. Med. Chem. 57* (7), 3126−3139.


https://dx.doi.org/10.1021/acsinfecdis.0c00472
*ACS Infect. Dis.* XXXX, XXX, XXX−XXX

(46) Labute, P. (2009) Protonate3D: Assignment of ionization states and hydrogen coordinates to macromolecular structures. *Proteins: Struct., Funct., Genet.* 75 (1), 187−205.
(47) Teng, K.-H., Hsu, E.-T., Chang, Y.-H., Lin, S.-W., and Liang, P.-H. (2016) Fluorescent Farnesyl Diphosphate Analogue: A Probe To Validate trans-Prenyltransferase Inhibitors. *Biochemistry* 55 (31), 4366−4374.
(48) Labute, P. (2008) The generalized born/volume integral implicit solvent model: Estimation of the free energy of hydration using London dispersion instead of atomic surface area. *J. Comput. Chem.* 29 (10), 1693−1698.
(49) Hanwell, M. D., Curtis, D. E., Lonie, D. C., Vandermeersch, T., Zurek, E., and Hutchison, G. R. (2012) Avogadro: an advanced semantic chemical editor, visualization, and analysis platform. *J. Cheminf.* 4, 17.


https://dx.doi.org/10.1021/acsinfecdis.0c00472
*ACS Infect. Dis.* XXXX, XXX, XXX−XXX